THESIS

MANUFACTURING AND TESTING OF SPLINE GEOMETRY USING CARBON FIBER REINFORCED COMPOSITE

Submitted by

Eric Jambor

Department of Mechanical Engineering

In partial fulfillment of the requirements

For the Degree of Master of Science

Colorado State University

Fort Collins, Colorado

Fall 2016

Master's Committee:

Advisor: Thomas Bradley

Donald Radford
Paul Heyliger

ABSTRACT

MANUFACTURING AND TESTING OF SPLINE GEOMETRY USING CARBON FIBER REINFORCED COMPOSITE

A model and manufacturing process for the design of carbon fiber reinforced composite spline shafts is developed and validated to investigate the feasibility of using composite splines for use in power transmission applications. Composite torque tubes for power transmission have been employed in various industries for over three decades and have shown up to a 50% mass decrease compared to steel shafts designed for the same use. One limiting factor for the amount of weight reduction achievable is the mechanism used to transfer power to and from the composite tube. Most composite shafts use adhesive bonding, fasteners, press fits, or some combination to join a steel or aluminum yolk or spline to the end of the tube. This research will investigate the feasibility of eliminating these mechanisms by replacing them by molding in splines to the composite torque tube. This will additionally reduce part count and manufacturing time as well as eliminating the heavy metal inserts. To achieve this, an analytical model is developed to investigate the strength of composite spline teeth of involute geometry as well as a composite torque tube. Due to the complex nature of designing with composites these models are supplemented by material models using a composite software package and finite element models (FEM). The involute splined shaft was then manufactured using an iterative approach to refine the sample quality and tested in torsion to failure. Although the peak failure torque had a large range over the samples it can be concluded that with improvements in the manufacturing process using molded composite splines is a feasible method of torque transfer. This can be concluded from the failure modes of the splined shaft as they indicate that the splines were able to adequately transfer the load to the torque tube.

ACKNOWLEDGEMENTS

This research has been supported in part by the United States Department of Energy and General Motors Advanced Vehicle Technology Competition: EcoCAR 3. Additional funding for this project has also come through the National Science Foundation through their sponsorship of the innovation portion of the EcoCAR 3 program. Special thanks go out to Dr. Thomas Bradley and Dr. Donald Radford of Colorado State University for the continuous support they have provided for me and this project.

TABLE OF CONTENTS

ABSTRACT ii
ACKNOWLEDGEMENTS iii
LIST OF TABLES vi
LIST OF FIGURES vii
LIST OF SYMBOLS ix
LIST OF EQUATIONS xi
INTRODUCTION 1
Climate Change and the Automotive Industry 1
Methods of Power Transmission 2
Splined Shafts 3
Composites in Splines 7
Thesis Objectives 9
Thesis Scope 10
MODEL AND DESIGN DEVELOPMENT 11
Design Criteria 11
Geometric Spline Model 12
Spline Load Analysis 15
Torque tube analysis 19
Material Design 21
Reinforcement 22
Matrix 29
Laminate Properties 30
Spline Shaft Revisited 33
FEM 34
Solid Body Modeling 34
Meshing 35
Laminate Model 37
FEM Assembly 38

FEM Results 40
SPLINE SHAFT MANUFACTURING 43
Phase One 43
Material Preparation 43
Lay-up Process 46
Phase Two 48
Phase Three 50
Post Processing 52
TESTING 54
Fixture Design Criteria 54
Fixture Design 55
Measurement 57
Testing 58
RESULTS 59
Data Set 59
Failure Modes 60
CONCLUSIONS 63
REFERENCES 66
APPENDIX 68
A: Spline Data 68
B: Reinforcement Data 69
C: Matrix Data 70
D: Fixture Design 71

LIST OF TABLES

Table 1: Calculated spline dimensions 13
Table 2: Generalized properties of various fibers [4] 23
Table 3: Calculated outer diameters of each fiber layer 26
Table 4: Calculated braid properties 28
Table 5: Calculated properties for TR30s Biaxial Braid 32
Table 6: Torsion test results in Nm; 4x multiplier with no derating 60
Table 7: Spline Data 68
Table 8: Various reinforcement properties used 69
Table 9: Epon 828/3140 unfilled casting data 70

LIST OF FIGURES

Figure 1: Torsional load distribution on splined shafts 3
Figure 2: Generation of involute profile on unit circle 4
Figure 3: Four main gear diameters 5
Figure 4: Pressure angle example 6
Figure 5: Varying pressure angles for a given base circle [13] 6
Figure 6: Hexagonal torque tube geometry [15] 8
Figure 7: Spline design, 13 tooth 8/16 DP 30° PA 10
Figure 8: Solid model showing the tooth body (teal) and tube body (tan) 14
Figure 9: Hertz stress of parallel cylinders in contact 15
Figure 10: gear contact (a) and distributed load on spline (b) 16
Figure 11: Uniform pressure distribution over spline tooth face 17
Figure 12: Approximation of tooth profile using rectangles [12] 18
Figure 13: Nominal diameter biaxial braid fiber orientation 25
Figure 14: Nominal 2D Braid Model 27
Figure 15: End view of solid body with simplified geometry for analysis 35
Figure 16: Tooth mesh face (a) and swept mesh (b) 36
Figure 17: Lay-up coordinate system 37
Figure 18: Splined coupling with mesh 39
Figure 19: Full FEM assembly 39
Figure 20: Visual scaled displacement of the splined shaft 41
Figure 21: Solid laminate failure index for ply 4 of the torque tube body 41
Figure 22: Interlaminar failure index of the spline teeth to the body using the bond strength of the epoxy 42
Figure 23: Trapezoidal approximation 44
Figure 24: Internal bagging tape 45
Figure 25: Lay-up kit 46
Figure 26: Molding compound charges 49
Figure 27: Phase two sample with poor surface finish and voids (red circle) 50
Figure 28: Sample from phase three manufacturing 51
Figure 29: Composite in tooling 52
Figure 30: Post processed splined shaft with interiorly angled teeth 52
Figure 31: Sample A15 after testing showing spline damage (green), main tube failure (red), and porosity (yellow) 60
Figure 32: Sample A11 after testing showing separation of teeth from body (green) 61
Figure 33: Sample A20 after testing showing fractures in teeth (red) 62
Figure 34: Predicted biaxial braid behavior when co-molded with tooth 64

Figure 35: Full test fixture assembly CAD (not pictured are bolts mating hex stock to applicator coupling) 71

LIST OF SYMBOLS

Symbol	Description	Units
a	Long side of approximation rectangle	[m]
A	Area	[m^2]
$A_{t,r}$	Contact area of tooth root	[m^2]
b	Short side of approximation rectangle	[m]
CF	Resultant contact force	[N]
DP	Diametral pitch	[teeth/in]
dp	Pitch diameter	[m]
D_{ri}	Major shaft diameter	[m]
E_c	Young's modulus of composite	[Pa]
E_f	Young's modulus of reinforcement	[Pa]
E_m	Young's modulus of matrix	[Pa]
F	Force	[N]
F_{pr}	Resultant force pitch radius	[N]
g	Gravitational constant	[m/s^2]
G	Shear modulus	[Pa]
G_c	Shear modulus of composite	[Pa]
G_f	Shear modulus of reinforcement	[Pa]
G_m	Shear modulus of matrix	[Pa]
G_{rr}	Shear modulus of torque tube	[Pa]
G_{tr}	Shear modulus of tooth	[Pa]
J	Polar moment of inertia	[m^4]
k_r	Torsional stiffness of splined shaft	[N•m^4]
$k_{r,r}$	Torsional stiffness of torque tube	[N•m^4]
$k_{t,r}$	Tooth stiffness	[N•m^4]
L	Length	[m]
l_c	Length of tooth	[m]
l_f	Length of tooth face	[m]
m	Module	[mm pitch diameter/tooth]
m_{veh}	Vehicle mass	[kg]
N	Tooth number	[-]
NC	Resultant contact force	[N]
N_{diff}	Differential gear ratio	[-]
Np	Number of plies	[-]
N_{trans}	Transmission gear ratio	[-]
PA	Pressure angle	[deg]
P_c	Uniform contact pressure	[Pa]
Pn	Circular pitch	[m]

r	Radius	[m]
r_b	Base circle radius	[m]
r_{wheel}	Wheel radius	[m]
T	Torque	[Nm]
t	Torque tube thickness	[Nm]
$T_{axle\_friction}$	Torque at axle using friction model	[Nm]
T_{axle_pinned}	Torque at axle using pinned model	[Nm]
T_{cap}	Torque capacity	[Nm]
T_{eng}	Torque produced by engine	[Nm]
T_{loss}	Torque losses	[Nm]
T_{motor}	Torque produced by motor	[Nm]
t_p	Ply thickness	[m]
V_f	Fiber volume fraction	[-]
V_m	Matrix volume fraction	[-]
V_v	Void volume fraction	[-]
z	Diameter-module relationship	[-]
β	Torsional cross section approximation	[-]
γ	Shear strain	[mm/mm]
θ_t	Angle of base circle occupied by tooth root	[rad]
λ	Angle of twist per unit length	[rad/m]
μ_{wheel}	Coefficient of friction at wheel	[-]
ν_c	Poisson's ratio of composite	[-]
ν_f	Poisson's ratio of reinforcement	[-]
ν_m	Poisson's ratio of matrix	[-]
π	Numerical value pi	[-]
ρ_c	Density of composite	[g/cm^3]
ρ_f	Density of reinforcement	[g/cm^3]
ρ_m	Density of matrix	[g/cm^3]
ϕ	Angle of twist	[rad]

LIST OF EQUATIONS

Equation 1: Torque capacity [15] 7
Equation 2: Axle torque for a pinned model 12
Equation 3: Axle torque for a friction model 12
Equation 4: Diametral pitch and module (m) relationship [11] 12
Equation 5: Circular pitch (P_n) and module relationship [11] 12
Equation 6: Pitch diameter (d_p) and module relationship [11] 12
Equation 7: Base circle radius (r_b) and pressure angle relationship [8] 12
Equation 8: Contact area of tooth root (A_{tr}) and torque tube body 15
Equation 9: Resultant force at pitch radius 17
Equation 10: Uniform contact pressure on tooth flank 17
Equation 11: Torsional stiffness of splined shaft 18
Equation 12: Applied torque relationship for rectangle 19
Equation 13: Calculation for β 19
Equation 14: Spline teeth torsional stiffness 19
Equation 15: Polar moment of inertia for thin walled tube 20
Equation 16: Torsional stiffness of a shaft 20
Equation 17: Tube thickness of a composite tube 20
Equation 18: Shear strain 21
Equation 19: Fiber orientation relationship 27
Equation 20: Area relationship 28
Equation 21: Rule of Mixtures 30
Equation 22: Rule of mixtures: density 30
Equation 23: Rule of mixtures: Young's modulus 31
Equation 24: Rule of mixtures: Poisson's Ratio 31
Equation 25: Rule of Mixtures: shear modulus 31

INTRODUCTION

Climate Change and the Automotive Industry

One of the largest issues facing the world today is climate change due to greenhouse gas (GHG) emissions, and in the U.S., the second largest contributor is the transportation sector [1]. Additionally Greene's report states that the transportation sector is the largest source of carbon dioxide (CO_2) and is larger than most countries total CO_2 output. The Environmental Protection Agency (EPA) has implemented policies to reduce U.S. GHG emissions from the transportation sector with various milestones leading up to a 55 mile per gallon (mpg) fleet average target by 2025 [2]. These targets are pushing manufacturers to come up with new strategies to reduce their corporate average fuel economy (CAFE).

There are a variety of ways to meet CAFE standards including vehicle electrification, creating more efficient systems, and reducing vehicle mass [1]. To reduce vehicle mass manufacturers have moved towards the use of lightweight materials such as aluminum alloys and composites [3]. Here composite materials will be discussed as fiber reinforcement, such as carbon or glass fiber, with polymer reinforcement like epoxy. Composite materials tend to have a very high specific strength and modulus which allows them to be used to create lightweight parts [4]. BMW has taken advantage of this with their I3 hybrid electric vehicle which utilizes carbon fiber reinforced composites to make up the majority of the vehicle [5]. This has allowed for both weight savings and a part reduction compared to a steel chassis. Other areas that have been targeted by composites are in the power transmission components.

Methods of Power Transmission

To propel themselves, vehicles use either an electric motor or an internal combustion engine to produce torque. Depending on the vehicle architecture this torque is transferred from the machine through a clutch or torque converter to a transmission. The torque is then multiplied by a gear ratio to achieve a desired output depending on the driver request. This torque is transferred through the transmission to an output shaft which typically leads to a rear differential (in the case of rear wheel drive vehicles) which splits power to each of the drive wheels [3]. As stated before, different architectures employ different mechanisms to transmit the torque to the wheels, but the general concept remains the same.

A critical component commonly found in many architectures is the drive shaft. This component is characterized by a shaft that is connected to the output of the transmission and runs down the longitudinal axis of the vehicle and supplies torque to the rear differential. Traditionally drive shafts have been made of steel so they could meet the common design requirement of 3500 Nm [6]. To meet the fundamental bending natural frequency these steel shafts were made in two pieces and connected with universal joints (u-joints). Drive shafts manufactured in this manner tend to be heavy, have multiple parts, and require multiple manufacturing processes [6]. To reduce vehicle weight and part count the first composite drive shaft was developed by the Spicer U-Joint Division of Dana Corporation for the Ford Econoline in 1985 [7]. Since then researches have explored the use of an aluminum tube and a combination of glass fiber epoxy composite and carbon fiber epoxy composite to achieve a single piece drive shaft that meets the design requirements [6], [7]. The research shows that a significant portion of the design was spent on the methods of transmitting torque in and out of the drive shaft.

To successfully transfer torque axially between components there must be some sort of coupling that allows movement and power transmission. As mentioned above this may be a friction plate, flexible coupling, or it could be a rigid coupling such as a splined shaft. Spline couplings are among the most common types of power transmission elements and are widely found in transmissions, axle joints, differential inputs, and even in clutches themselves [3], [8]. In the research conducted by Lee et al. a two part interface of small splines and adhesive bonding was used to connect u-joint yolks to each end.

Splined Shafts

Splined shafts in their simplest form are just keyed shafts [9]. Keyed shafts have limitations with their maximum torque due to stress concentrations in the keyway as well as transferring the entire load through a single spline. By adding teeth, or splines, radially around a shaft it is possible to reduce the load that each tooth carries [10]. The ideal case is illustrated in Figure 1 where a total of four splines carry 25% of the load. This is considered an ideal due to manufacturing defects on the spline coupling which cause misalignment between the shaft spline couple [10].

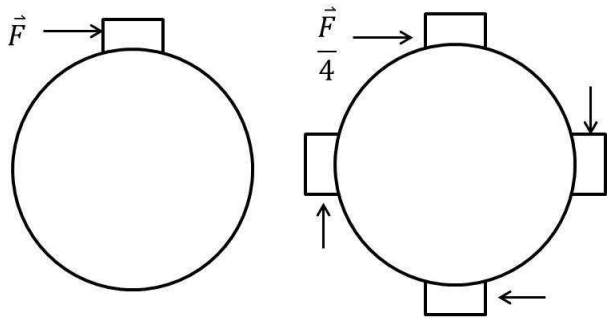

Figure 1: Torsional load distribution on splined shafts

Splined shafts, much like gears, have practical limitations on how many splines they can have and how that affects the interface with the coupling [11]. Many of these limitations are geometric and manufacturing based. For a given base diameter of a shaft there is a physical limitation to how many splines can be machined onto the face. Additionally Hayashi and Hayashi show that the torsional stiffness of the teeth is related to both the module (mm of pitch diameter per tooth) and diameter. As the stiffness decreases there will be a corresponding increase in torsional stress [12], [11].

As both gears and splined shafts have been developed throughout history a prevailing geometry has dominated the tooth profile. The profile that has been developed is called an involute curve and can be drawn by tracing the path of the end of a string as it is unwound from a base cylinder. This method of constructing the involute curve is shown in Figure 2. All of the construction lines that make up the segments of the involute curve are tangent to the base circle [8].

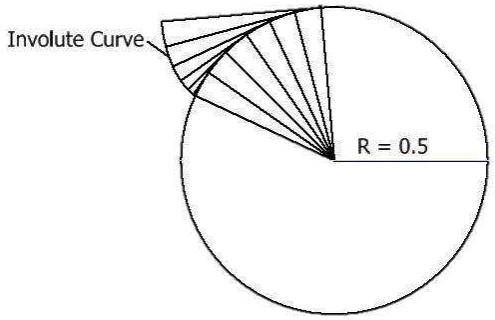

Figure 2: Generation of involute profile on unit circle

When extruded axially the involute profile generates the flank and face of the gear or spline tooth which is the area of the tooth that is contacted and used to transfer load [11]. When designing gears or splines and their interfaces, there are four circles that the other dimensions are based off: base circle, pitch circle, addendum circle, and dedendum circle (Figure 3) [8].

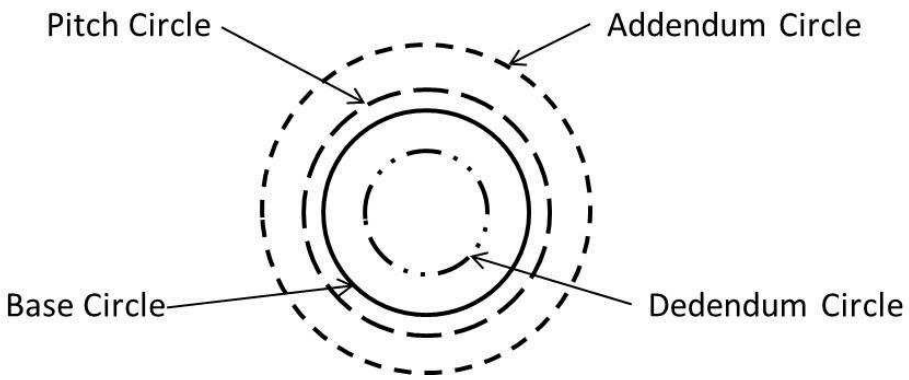

Figure 3: Four main gear diameters

The involute profile was originally design for gears because it allows for a continuous contact between gear teeth as well as a constant pressure angle. This creates a quieter gear meshing, can increase gear life, and can handle more torque than a straight sided tooth [10], [13]. Two other important terms that should be also be defined are pressure angle (PA) and diametral pitch. The pressure angle is the angle formed by drawing a line tangent to the base circles of a gear pairing and intersecting the pitch circles as shown in Figure 4. Pressure angles may vary, but common pressure angles for gears today are 20° and 25° and dictate what part of the involute is used [13]. Splines generally use a higher pressure angle such as 30°, 37.5°, and 45° [10]. The higher the pressure angle for a given base circle generates a larger pitch diameter and a wider tooth as seen in Figure 5. The diametral pitch is simply a measurement of the number of teeth per inch of pitch diameter. The SI designation for this is module and is millimeters of pitch diameter per tooth so tooth module is essentially the inverse of diametral pitch [11]. It is standard practice for spline teeth to use standard pitches such as 8/16 or 10/20, where the numerator is the diametral pitch and the denominator is the stub pitch which controls tooth height. Its measurement is the radial distance from the pitch circle to the addendum circle of the spline [14].

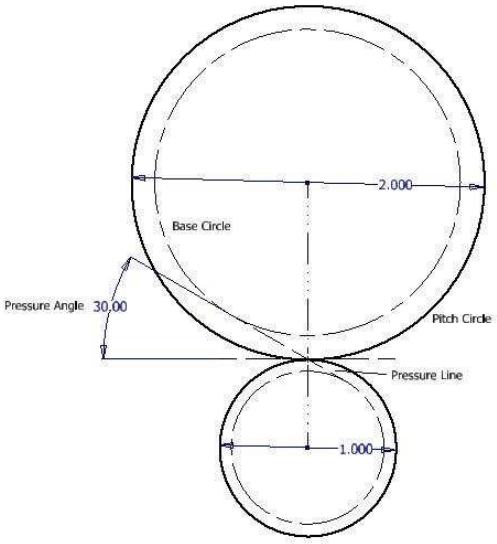

Figure 4: Pressure angle example

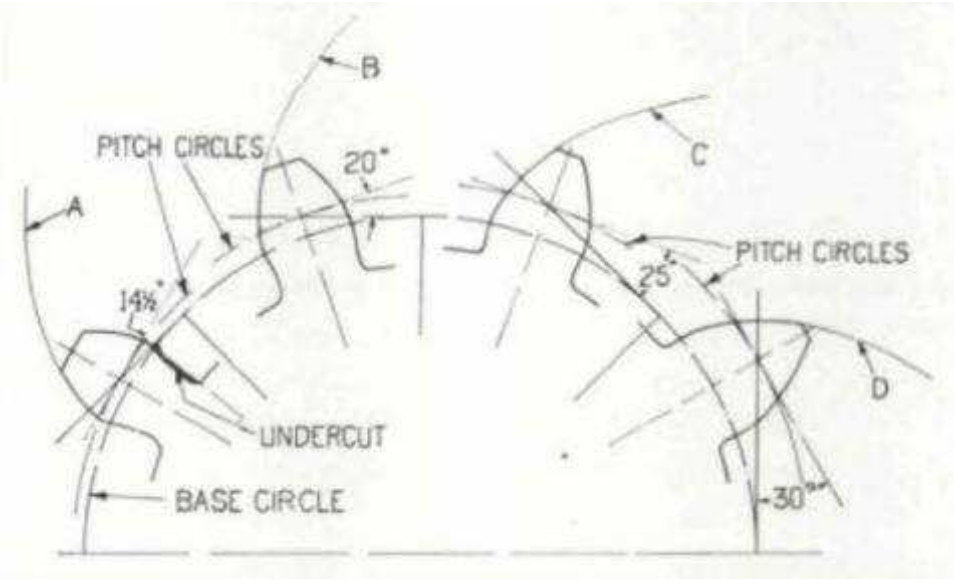

Figure 5: Varying pressure angles for a given base circle [13]

Composites in Splines

In 1995 Gross and Goree investigated the use of non-circular cross sections in composites to transfer torque in and out of a shaft. Their work is one of the fundamental building blocks of this research as it proved that fasteners and metal inserts could be avoided in composite torque transfer applications. Their research focused on the development of non-circular cross section geometry in composites to create a mechanical interference between the two mating parts so as to allow torque transfer. For a non-circular cross section the torque capacity is defined as:

Equation 1: Torque capacity [15]

$$T_{cap} = (CF)(L)(NC)$$

Where CF is the resultant contact force from the contact pressure distribution, L is the lever arm of the contact force applied at the line of action of the force applied at the centroid of the shape, and NC is the number of contact surfaces [15]. It is shown that for geometric shapes L and CF are related when the contact force is assumed to be normal to the vertices of the polygon. As with traditional spline shafts as the mating piece is rotated in the coupling it travels through a tilt angle which then allows the other teeth to begin engaging [16]. Although in splines this is generally modeled as a tooth distortion once the first tooth engages with the couple it is the same concept used by Gross and Goree. This concept is used to create correlation between maximum displacement and the length of the lever arm with the assumption that contact pressure is proportional to the magnitude of the normal displacement [15]. With their geometric and kinematic analytical models Gross and Goree tested a series of geometries, mainly of the trilobal type, using carbon fiber reinforced epoxy composites. Testing of these composites indicated that their failure torque was less than the failure torque of an ideal circular torque tube, which

was expected. The research indicated that increasing the contact points allowed the failure torque to approach the ideal failure torque. This led to the development of the hexagonal spline geometry seen in Figure 6. Since the geometry developed was an internal spline, the outer surface was reinforced with a carbon fiber composite overwrap and foam filler as shown by the outer circle in Figure 6. The torsional failure results of this design showed that the failure occurred in the transitional area of the spline to the circular torque tube and not in the end itself [15]. The conclusions of this research were that it would be feasible to use internal splined geometry with an overwrap to transmit torque if the transition section were properly designed and that failure torques of well over 70% of the ideal failure torque could be reached. Although the mechanics are very similar to external splines the overwrap and filler material were large contributors to the increase in failure torque. To mate to an existing internal spline, such as in a constant velocity joint (CV-joint) of an axle, an external spline would be needed. This geometry eliminates the ability to use an overwrap to increase torsional strength and must rely solely on the teeth to transmit torque.

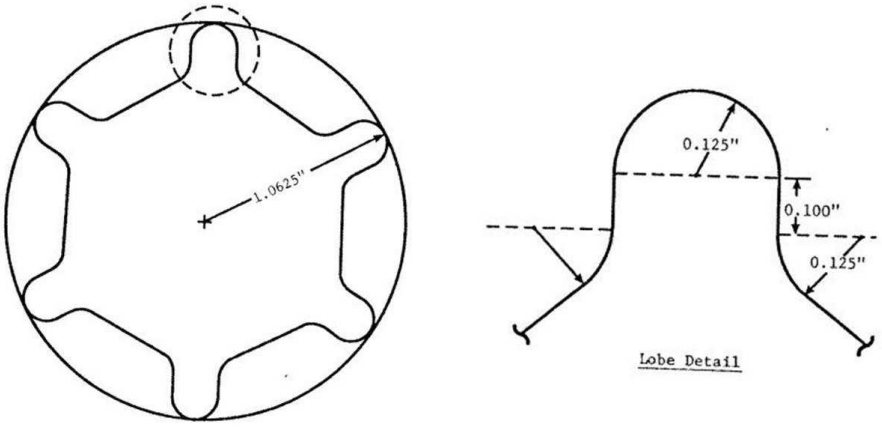

Figure 6: Hexagonal torque tube geometry [15]

Thesis Objectives

The goal of this thesis is to develop a model and manufacturing process for the use of carbon fiber reinforced polymer composites in an involute splined shaft. The model and manufacturing process will be compared to physical test results to determine if the approach is a feasible methodology for the design of composite splines. Additionally the thesis will investigate the feasibility of using composite splines as a method of power transmission so as to eliminate metal inserts and fasteners that are currently used. If feasible, composite spline applications could be far reaching in weight sensitive power transmission applications as well as in part count reduction. Application fields range from aerospace, automotive, and marine industries and if widely employed could lead to large and widespread design improvements. Since the geometry being used is for external splines, molds and couplings do not have to be designed as they already exist. A five step plan to achieve the objectives of this thesis is outlined below:

1. Develop design constraints
2. Develop models for the design of involute composite spline shaft
    a. Material model
    b. Analytical load model
    c. FEM model
3. Develop manufacturing process to achieve desired performance and geometry
4. Develop torsion test rig
5. Test samples to failure and analyze results

Thesis Scope

Due to lack of documentation on the generation of involute splined shafts using carbon fiber reinforced composites the scope of this thesis will be limited to one spline design. Although studies could be conducted to optimize the spline geometry for use with composite materials this research will focus primarily on the development of a design model for composite involute spline shafts, manufacturing, and validation. Limiting the design to a single spline shaft design reduces the amount of resources required for almost all aspects of the project. It also allows for a more thorough comparison to the design model and manufacturing process since all of the samples will be made to the same specifications. The spline shaft design, specifically, will use a 95.25 mm long, 13 tooth 8/16 diametral pitch (DP) and 30° pressure angle (PA) spline coupling with a 44.45 mm dedendum that is commercially available (Figure 7).

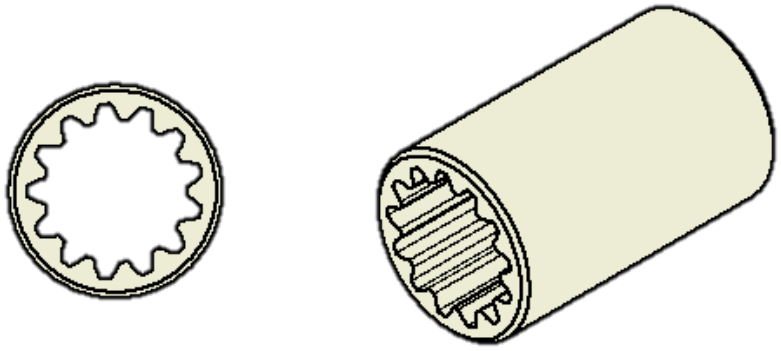

Figure 7: Spline design, 13 tooth 8/16 DP 30° PA

MODEL AND DESIGN DEVELOPMENT

This section will focus on the detailed design of the composite splined shaft and the model development necessary to support the design.

Design Criteria

To develop design models it is necessary to know the design criteria [4]. Since one of the targeted application areas for a composite spline shaft is at the axle it would be ideal to design to the load scenarios seen here. Depending on the model used to calculate axle torque, whether it is the sum of the torques across the entire powertrain (Equation 2) or a friction based model (Equation 3), the lower end total torques are upwards of 2700 Nm [17]. Due to limitations in available test equipment the maximum torsional load that is able to be applied is closer to 1000 Nm. This restriction also limits the ability to design to the transmission output torque as these are often designed to 3000 Nm [18]. This makes the next logical torque criteria the input to the transmission. Since this project is sponsored by the Advanced Vehicle Technology Competition: EcoCAR 3, it was decided to use the torque input of the 2016 Chevrolet Camaro being converted into a hybrid electric vehicle at Colorado State University. The maximum allowable torque input to the transmission used in this vehicle is 550 Nm which is within the test equipment range. This torque criterion will be used to appropriately size the torque tube which will be discussed later. Other design criteria are the geometric limitations as described in the scope of this paper. The selected geometry will limit the torque tube outer diameter, but not the inner diameter, which allows for different ply counts to be used in the design. The spline teeth are completely geometrically constrained as they are bounded by the coupling shown in Figure 7 and the torque tube shown in Figure 8. Since the teeth are fully bound the design parameters are limited to material selection and manufacturing processes.

Equation 2: Axle torque for a pinned model

$$T_{axle\_pinned} = (T_{eng} + T_{motor}) * N_{trans} * N_{differential} - T_{loss}$$

Equation 3: Axle torque for a friction model

$$T_{axle\_friction} = g * m_{veh\_distributed} * \mu_{wheel} * r_{wheel}$$

Geometric Spline Model

As discussed in the scope of this research the geometry of the involute spline was selected and will be held constant. This significantly reduces the amount of work required as the involute spline geometry does not need to be developed from scratch, rather just fully understood. As stated before the geometry selected is a 13 tooth 8/16 DP 30° PA splined coupling with a major diameter (dedendum) of 44.45mm. To understand the rest of the dimensions of the spline a series of geometric relationships are defined.

Equation 4: Diametral pitch and module (m) relationship [11]

$$DP = \frac{25.40}{m}$$

Equation 5: Circular pitch (P_n) and module relationship [11]

$$P_n = m * \pi$$

Equation 6: Pitch diameter (d_p) and module relationship [11]

$$d_p = N * m$$

Equation 7: Base circle radius (r_b) and pressure angle relationship [8]

$$r_b = \frac{d_p}{2} * \cos\phi$$

Based on these geometric relationships several crucial dimensions can be calculated given only the diametral pitch and tooth number (N). Table 1 shows the values calculated for the spline coupling that will be used for this research.

Table 1: Calculated spline dimensions

Dimension	Value (mm)
Module (m)	3.175
Circular Pitch (P_n)	9.970
Pitch Diameter (d_p)	41.275
Dedendum (h_f)	44.45
Base Circle Radius (r_b)	17.823

The dimensions listed in Table 1 make it possible to create a solid model of both the spline coupling and splined shaft. This is a critical first step in developing different finite element models. To generate the solid models the design accelerator tool in Autodesk® Inventor® was used. This tool allows for the automatic generation of both parallel and involute splines. It can be applied to both internal and external splines. To use this tool appropriately it is necessary to know the dimensions in Table 1 so that the generated dimensions can be cross referenced to the calculated dimensions. There are various standard templates used in industry for both gears and splines and without knowing the standards to which the purchased coupling was manufactured to, the dimensions need to be cross referenced to ensure accuracy. Choosing the wrong template can change the major diameter and other dimensions by over 3mm. The full spline dimensions are listed in Table 7. Using this model it is possible to measure the arc length of the involute, or flank (l_f) in the software. This dimension was found to be 4.93mm and will be used to find total contact area.

To use the solid model as an effective base for the finite element model it is necessary to create two separate solid bodies in the same model. The solid bodies, shown in Figure 8, consist of the teeth depicted in teal and tube depicted in tan. Generating the solid model in this way allows for a variation in

the tube thickness to account for different composite ply counts as well as the ability to customize the mesh used in the laminate modeling. The geometry shown in Figure 8 has been idealized by removing the small fillet radii along the length of the teeth. Idealizing the geometry in this manner, as will be discussed in more detail, allows for reduced computational time in the FEM and for better mesh generation.

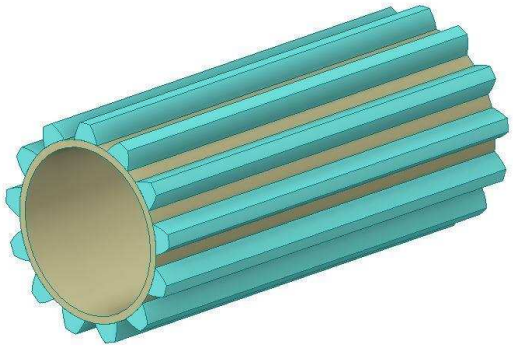

Figure 8: Solid model showing the tooth body (teal) and tube body (tan)

The definition of two different bodies in the solid model leads to an assumption made for the rest of the analysis: the splined shaft can be modeled as a tube body modeled as a torque tube and of spline bodies fixed to the torque tube. This assumption is supported by Hayashi and Hayashi who created a load model for splines by separating the spline teeth from the body in their calculations [12]. This assumption splits the design problem into two fundamental pieces. Since the torque is transferred from the shaft from the coupling by way of the teeth the first part is to ensure that the teeth are designed so that they can adequately transfer these loads into the body. The second portion is to design the torque tube so that it can withstand the desired loads assuming the teeth are able to transmit the full load into the body. With an isotropic material such as steel these assumptions have little impact since the entire body is a single piece machined from a blank. Utilizing composites, however, the manufacturing method plays a critical role in ensuring a solid bond between the teeth and torque tube.

The bond area can be calculated using Equation 8 where θ_t is the angle in degrees of the base circle occupied by the tooth root. Depending on where the fillet radius is included in the measurement θ_t ranges from 20.46° (without fillet) to 21.58° (with fillet). For future calculations the θ_t will be 21.58°.

Equation 8: Contact area of tooth root (A_{tr}) and torque tube body

$$A_{tr} = r_b * \theta_t * l_c$$

Spline Load Analysis

The load of an involute gear tooth is generally considered to occur along a pressure line that moves as the gears move through their rotation [19], [8]. This contact can be modeled as hertz stresses along the faces of the meshed gears where the gear faces are modeled as parallel cylinders as shown in Figure 9 [11].

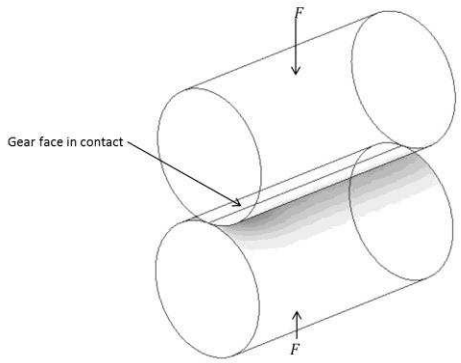

Figure 9: Hertz stress of parallel cylinders in contact

Splines differ from this model since the teeth of the shaft are in full mesh with the teeth from the spline couple [19]. In Figure 10 (a) the shaft couple interface is shown from the solid model along with (b) the distributed load on the flank of the tooth [19]. In this model the resultant force shown in red is applied at the pitch circle radius. This is not a perfect model as described by Cura and Mura since the actual distributed force (green) is not uniform across the flank of the spline. The dissymmetric pressure

distribution can be modeled using a modified punch model by dividing the tooth into increments along its height [16]. The results of Cura and Mura's research, however, indicate that using a non-uniform distribution model with a new resultant force application radius only yields a difference of 0.85% at a 500 Nm torque when compared to the original pitch radius.

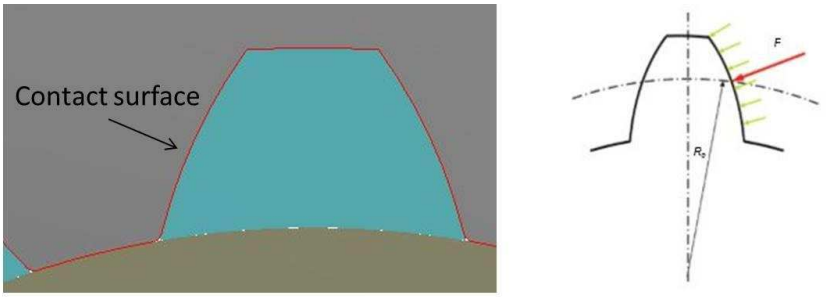

Figure 10: gear contact (a) and distributed load on spline (b)

Since the load case for the composite system is 550 Nm it is reasonable to assume that there will be a similar error in resultant force location radius. Since the error is so small, especially when compared to the error in estimating composite material properties (as will be discussed later), the resultant force of the contact forces along the flank will be applied at the pitch radius perpendicular to the profile. Since this is the resultant force due to an evenly distributed pressure over the tooth flank it can be concluded that it is also reasonable to model the distributed contact pressure across the flank of the tooth as uniform. Additional support for this assumption refers back to the criteria development where many of the design properties of the spline teeth are fixed. Since the tooth depth, thickness, and pressure angle will not change during this research there is a reduced benefit in understanding the small differences between uniform and non-uniform pressure distributions.

Using the geometry calculated above and from the solid model and the assumption that the resultant force acts at the pitch radius then Equation 9 can be developed where F_{pr} is the resultant force

applied at the pitch radius and T is torque. For this specific design T is 550 Nm which produces a 26.7 kN value for F_{pr}. Using the assumption that the resultant force is generated by a uniform pressure across the tooth flank the pressure can be calculated using Equation 10 where P_c is the uniform contact pressure and l_f is the length of contact along the face of the tooth. Due to the test rig geometry there is a maximum contact length of 31.75 mm. Using this length the resulting uniform pressure is 170.26 kPa. This can then be divided by the total number of splines to give a total pressure of 13.1 kPa per spline.

Equation 9: Resultant force at pitch radius

$$F_{pr} = \frac{T * d_p}{2}$$

Equation 10: Uniform contact pressure on tooth flank

$$P_c = \frac{F_{pr}}{l_f * l_c}$$

The applied uniform pressure over the spline tooth can be seen in Equation 10. This is a representation of how much the torque applicator coupling will engage with the composite spline test sample. The entire face in contact is modeled as having applied pressure since the coupling geometry is the same as the mold geometry. This provides a light press fit effect which is different than many spline couple interfaces that have a fairly loose slip fit.

Figure 11: Uniform pressure distribution over spline tooth face

With these assumptions established it is possible to calculate the shear stress in the tooth, which is of ultimate interest, since shear from the teeth into the torque tube will dictate the torque tube design. It is also of interest since it establishes and analytical value for shear stress that can then be compared to the FE model as well as be compared to the allowable shear stress of the composite material to give an estimate for the torsional upper limit that the teeth can handle. The upper torsional limit will give an understanding of the application range for this design.

To calculate shear stress in a spline tooth various models have been developed based on approximations of the tooth profile. One of the most straight forward models is assuming the tooth behaves like a cantilever beam [11]. If this assumption is made then a rectangle can be drawn that approximates the tooth profile as shown in Figure 12 [12]. Using this assumption Hayashi and Hayashi continue their model by assuming that the torsional stiffness of the system is the sum of the torsional stiffness of the teeth and the torsional stiffness of the shaft minus the teeth. This is shown in Equation 11 where k_r is the stiffness of the whole shaft, $k_{t,r}$ is the stiffness of the teeth, and $k_{r,r}$ is the torsional stiffness of the shaft without the teeth [12].

Equation 11: Torsional stiffness of splined shaft

$$k_r = k_{t,r} + k_{r,r}$$

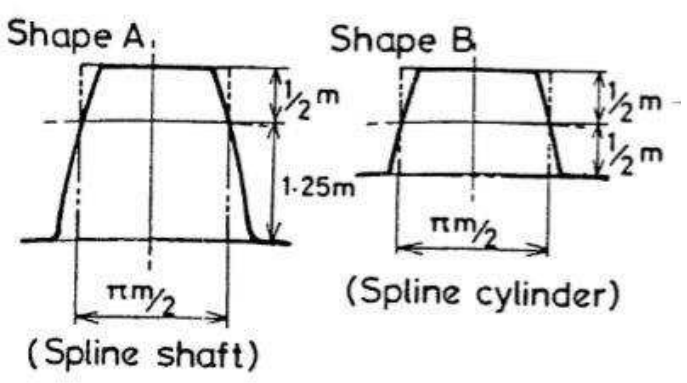

Figure 12: Approximation of tooth profile using rectangles [12]

Using the rectangular approximation the torque, T, can be related to angle of twist per unit length (λ) through Equation 12. In this equation G is the shear modulus and βab^3 represents the torsional cross section where β is calculated in Equation 13 and a and b are the long and short sides of the rectangular approximation, respectively [12].

Equation 12: Applied torque relationship for rectangle

$$T = \beta a b^3 \lambda G$$

Equation 13: Calculation for β

$$\beta = (\frac{1}{3} - .21\frac{b}{a}\left(1 - \frac{b^4}{12a^4}\right))$$

The dimensions for the rectangle are then approximated using the dimensions listed in Figure 12 where a = 1.75m and b = π/2m and m is the module. Hayashi and Hayashi then substitute the module related values for a and b along with the major shaft diameter (D_{ri}) and the number of teeth using the relationship of $D_{ri} = m(z+1)$ to get a to a final equation for total torsional stiffness of the teeth (Equation 14). To calculate the torsional stiffness the shear modulus of the teeth ($G_{t,r}$) will need to be calculated which will be developed in a later section.

Equation 14: Spline teeth torsional stiffness

$$k_{t,r} = \frac{1.051z}{z+1} D_{ri}^4 G_{t,r}$$

Torque tube analysis

The torque tube portion of the composite spline is modeled separately from the splines since the material properties differ between the splines and tube with the assumption that the splines will transfer all of the loads into the torque tube. The composite torque tube can be modeled as a thin wall tube since the thickness of the tube wall is significantly smaller than the radius of the tube [20]. Using

the polar moment of inertia for a tube, given as J in Equation 15, and the equation for generalized stiffness of a shaft (Equation 16) the torsional stiffness $k_{r,r}$ can be solved, where ϕ is the angle of twist. When solving for J, r is the mean radius and t is the thickness of the tube.

Equation 15: Polar moment of inertia for thin walled tube

$$J = \frac{\pi}{2}(r^4 - (r-t)^4)$$

Equation 16: Torsional stiffness of a shaft

$$\frac{T}{\phi} = \frac{G_{r,r} * J}{L}$$

This can't be solved at this time since the thickness of t is dependent on the ply structure of the composite tube which is a variable of the design. The thickness of the tube is defined by Equation 17 where N_p is the number of plies used and t_p is the thickness of a single ply.

Equation 17: Tube thickness of a composite tube

$$t = N_p * t_p$$

$G_{r,r}$, the shear modulus of the tube is also currently undefined since the material and ply structure will change the final value. The next step is to determine the maximum allowable angle of twist. Since most carbon fibers have a maximum strain of 1-2% it is possible to determine the maximum angle of twist without exceeding the allowable strain [4]. The maximum strain for a shaft in torsion will occur at the largest radius of the tube, this is also the location of the greatest angle of twist [20]. As will be discussed later, fibers oriented at ±45° to the tube axis are loaded axially in pure torsion. This means that the shear strain is the axial strain for these fibers. Equation 18 gives the relation of shear strain to the change in angle of twist (Δϕ, rads) and tube geometry. Given that most carbon fibers have a max tensile strain of 1-2% the angle of twist for the given tube geometry can range from roughly 3-6 degrees.

Equation 18: Shear strain

$$\gamma = \frac{r_{tube*\Delta\phi}}{l_{tube}}$$

For this design a maximum angle of twist of 4° will be used. This should ensure that the strain due to the torsional load in the outer ply is about 1.4%, which is within the allowable strain given in Table 8 for the material used. Using 550 Nm as a value for T, Equation 16 can be solved for $G_{r,r}$*J which gives a result in units of pressure. Once the shear modulus for the shaft material is determined the thickness of the tube, t, and the number of plies needed can be solved.

Material Design

When using composites the designer has the flexibility to tailor the constituent materials to achieve a desired overall property. This section of the design phase is critical because it determines the final physical properties of the composite. Depending on the material selection a wide array of properties can be achieved such as high stiffness, chemical resistance, impact resistance, and electrical resistance. The shear modulus, which is important for the torque tube design, is also controlled by the constituent materials. For the composites used in this research the constituent materials consist of a matrix and reinforcement, generally a fiber. The matrix, which is generally a thermoset or thermoplastic, depending on the manufacturing methods and use cases, transfers load between the fibers through shear. The fibers then carry the majority of the load in the composite.

Reinforcement

There are a variety of fibers that are commercially available for use in composites. These range from naturally occurring fibers such as flax to developed materials such as aramids, carbon/graphite, and glass fibers. The large variety in fibers types gives the designer a large design freedom with the tradeoff of having so many choices it can take a considerable amount of time to select the appropriate material, especially when there are so many variations between manufacturers. To help down select material for this project the fiber type was selected by comparing the product requirements to the relevant fiber properties.

The three main fiber types that were readily available were glass, carbon, and aramid. Glass fibers are by far the cheapest of the three types and have high insulative properties. This makes them a good candidate for applications needing electrical isolation, chemical resistance, and in designs that will have metal hard points or inserts in contact with the fibers [4]. Since carbon fibers are conductive they tend to cause galvanic corrosion when in contact with metals. This can cause significant design issues if bolts or bonded metal parts are used with carbon fibers. Since the design does not allow for direct contact with the fibers (they are insulated by the resin) carbon fibers remained a viable option.

Examination of the physical properties of glass fibers shows that the tensile modulus ranges from approximately 65-83 GPa depending on the type of glass [4]. In comparison the carbon/graphite fibers tend to have both a higher modulus and tensile strength than glass or aramid fibers as well as higher specific strength and modulus. The only exception is when comparing the tensile strength of S-glass with standard and ultra-high modulus graphite and the aramid fibers. S-glass, however, is significantly more expensive and harder to find in a variety of forms than its counterpart, E-glass. These issues eliminated S-glass as a viable material for this research, but leave it as a possibility to explore in

future iterations of the design where a high strength insulating material may be necessary. Additionally the aramid fibers could also have application in future iterations due to its high impact strength and toughness. An outer layer of aramid fiber could increase the longevity in an actual on vehicle use scenario where there is impact potential.

Table 2: Generalized properties of various fibers [4]

Fiber Type	Density (g/cc)	Tensile Strength (MPa)	Tensile Modulus (GPa)	Elongation to Break (%)
E-glass	2.5	3447	69	4.9
S-glass	2.5	4585	83	5.7
Carbon/graphite (standard mod.)	1.8	4137	228	1.6
Carbon/graphite (intermediate mod.)	1.8	5378	276	1.8
Carbon/graphite (ultra-high mod.)	1.9	3447	441	0.5
Aramid (high toughness)	1.4	3606	83	4.0
Aramid (high mod.)	1.4	3999	131	2.8
Aramid (ultra-high mod.)	1.5	3406	186	2.0

Since this research was focusing on the torsional strength and manufacturing methods of a splined shaft carbon/graphite fibers were the primary choice. This proved to be a good option as there are a wide variety of readily available carbon and graphite fibers that come in many different fabrics, braids, and unidirectional sheets.

Since the composite is loaded in torsion the fibers were oriented so that their axis was aligned with the load axis as close as possible given the final material constraints. The ideal fiber axis would be ±45° from the longitudinal axis of the tube. In pure torsion this would have the effect of loading the fibers in tension/compression axially and maximize the properties of the fibers since they are much higher axially than transversely.

Spline Reinforcement

The design of the composite splined shaft essentially needed two types of manufacturing processes: one for the splines themselves and the other for the shaft body. Due to the relatively high angles within the splines of the mold short chopped fiber was chosen as the reinforcement to avoid breaking longer fibers in the manufacturing process. The randomly oriented fiber also acted as more of a pseudo-isotropic material allowing it to have fibers aligned with the loads that would be out of plane if a fabric was used. This design requires the load from the spline teeth to be transferred via shear to the rest of the shaft body through the root of the teeth. Fibers for this processes were located first from ACP composites in small scale to run test samples to ensure the functionality of the manufacturing process and once validated purchased in larger quantity from a more readily available distributor. When changing manufacturers the data sheets for the two types of chopped fibers were compared and found to have less than a 3% variation in listed properties. Both were standard modulus graphite fibers chopped to 0.25 in. in length.

Tube Reinforcement

The idea behind the separate cylindrical body is that long fibers could be oriented to handle the torsional loads much more effectively than a part completely made out of chopped fiber epoxy composite. Since pure torsion loads the tube in a 45° helical direction around the tube the ideal fiber placement is to run fibers in line with these loads (±45° from the longitudinal axis). This method of fiber placement utilizes the full axial strength and stiffness of the fibers as previously mentioned.

To actually achieve this fiber orientation presents a number of problems due to the tooling geometry and other manufacturing processes. Since the internal diameter of the mold is approximately

38mm not counting the teeth (as they are filled with chopped fiber) the working area is very small to perform hand lay-up. Additionally the teeth are filled with wetted out fiber before the tube body is made and then they are co-cured under vacuum to create a sufficient bond. This means that the hand lay-up of the tube needs to be done in a manner so as to avoid shifting the chopped fibers in the teeth. It is also desirable to have continuous fibers throughout the entire tube (no cut lines) so that it acts as a complete unit and has fewer stress concentrators. Finally since it is an internal mold traditional methods of generating tubes such as filament winding are not applicable, at lease with the equipment available at CSU, further limiting material choice for this section of the design.

All of these challenges tend to point to a common solution: carbon fiber biaxial braid. Biaxial braid is often compared to a Chinese finger trap. Continuous fibers are braided together to form a tube with a nominal diameter. At nominal the fibers lay at ±45° to the longitudinal axis as shown in Figure 13.

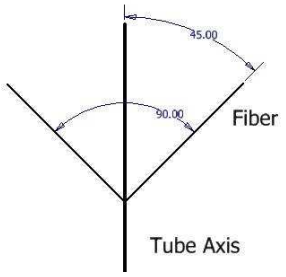

Figure 13: Nominal diameter biaxial braid fiber orientation

Since the fibers are free to shift in relation to each other within a set of constraints the braided tube can change diameters and length. By increasing the tube diameter from nominal, the fibers move towards the hoop direction, or 90° from longitudinal. This also causes the overall length of the section of braid to decrease. Decreasing the tube diameter has the opposite effect for fiber orientation and length. Using biaxial braid to generate a composite tube means there will be multiple layers of braid unless the tube is manufactured from a single layer. This necessarily means that every layer will have a slightly different fiber angle, length, and diameter as the part thickness changes with each layer of braid used.

Braid with a nominal diameter of 38.1 mm (1.5 in.) is commonly available through a variety of suppliers. This suites the geometry of the mold since the internal addendum is 38.1 mm (Table 7) which allows for the outer layer of the tube section to have a fiber orientation of ±45°. This is critical in increasing torque capacity since the outer layers carry higher load which means fiber angle is even more important in this area. The thickness of the fiber with a 50% fiber volume fraction (V_f), which will be discussed later, is listed as 0.33mm from the manufacturer. Since the braid is tubular the total change in diameter is double the fiber thickness or 0.66mm as shown in Table 8. As each layer's diameter decreases the fiber angle must also decrease. To understand how the fiber angles change given changing diameter and length a fiber model was built.

Table 3: Calculated outer diameters of each fiber layer

Layer	Diameter (mm)
1	38.1
2	37.44
3	36.78
4	36.12

Fiber Model

The fiber model approaches the problem by following the orientation of a single fiber around the braided tube since this is how the actual fiber is oriented. It is possible to break the 3D helical fiber path into a 2D path by making an imaginary cut along the braids longitudinal axis and laying it in a 2D plane. Mapping a fiber that originates at the center of the unfolded segment gives the total fiber path. This is demonstrated by the red lines (c1, c2) in Figure 14 which are at a 45° angle in the figure.

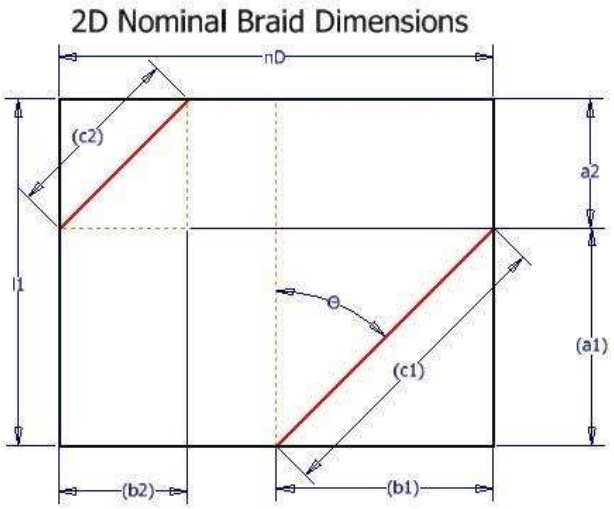

Figure 14: Nominal 2D Braid Model

To develop a geometric relationship between the changing diameter and fiber angle the assumption that the fibers move relative to the change in length must be made. This assumption assumes that all of the fibers shift by the same fiber angle during elongation, which in practice can change, especially if the mold has changing diameters. This allows for Equation 19 to be used which essentially states that the length of $a_{1,1}$, which is the length of a_1 from Figure 14 at the nominal diameter (diameter 1, Table 8).

Equation 19: Fiber orientation relationship

$$\frac{a_{1,1}}{l_1} = \frac{a_{1,x}}{l_x}$$

Another assumption that is made is the total area covered by the braided fabric is constant. This means that the nominal diameter and length determine the base area which remains constant throughout the dimensional changes. This relationship is given by Equation 20 where D_1 and l_1 are the nominal diameter and length respectively. This allows for the calculation of the length of the 2D geometry in Figure 14 for any given change in diameter. The calculated lengths are given in Table 4.

Equation 20: Area relationship

$$A = \pi * D_1 * l_1$$

Finally the last assumption is that the fiber in question stems from the center of the braid and does not shift laterally. This means that the starting location of line c1 in Figure 14 always starts at the midpoint of the rectangle. These three relationships allow for the calculation of the angle theta which is given in Table 4. Table 4 shows an increase in braid length which is accurate given a starting base length, however in manufacturing the excess length is trimmed causing each layer to have a shorter nominal length. This does not affect the fiber angle because the fiber angle is essentially fixed for any given braid diameter based on the previous assumptions. The predicted change in mechanical properties due to fiber orientation shows around a 2-3% decrease in shear modulus with the decrease in fiber angle [4], [21]. Since there is a relatively small decrease in properties all four layers will be assumed to have the same physical properties.

Table 4: Calculated braid properties

Layer	Length (mm)	a_x (mm)	Θ (deg)
1	95.25	59.85	45
2	96.93	60.90	44.00
3	98.67	62.00	42.98
4	100.47	63.13	41.64

Matrix

Matrix material encapsulates the fibers and allows the loads to be transferred throughout the entire laminate. There are a wide variety of matrix materials available for use with composites the most common being polyesters, vinylesters, and epoxies all of which are thermosets. Unlike thermoplastics, thermosets can't be reprocessed by heating them up passed their processing temperature. Overheating of thermosets leads to degradation and eventual breakdown. Epoxies tend to have higher mechanical properties than polyesters and vinylesters leading to its use in this research.

Epoxies function as a two part resin and hardener system that when combined begin a crosslinking or curing process. To maximize the mechanical properties the correct ratio of resin to hardener must be used. This is because there are a specific amount of bond sites and having too much or too little hardener will result in open bond sites which reduce the crosslink density [4].

Due to its relatively good properties, ease of use during the manufacturing process, and availability in the lab, the Epon 828/3140 resin hardener system was used. The curing agent, or hardener (3140), is a polyamide. The cure cycle for this system ranges from approximately 4 days at room temperature to one hour at a 100° C [22]. The properties as well as the cure cycle vary depending on the parts per hundred (phr) of curing agent to resin. The stoichiometric ratio, which tends to maximize most mechanical properties due to the high cross-link density achieved is listed as 33 phr [22]. The literature also shows that a majority of the mechanical properties are also significantly higher if a heated cure is used. Due to empirical evidence once the manufacturing process was started a short room temperature cure (approximately 6-8 hours) was used to remove voids followed by a 1 hour 100° C second stage heated cure. This process increased the surface finish and lowered the void content significantly while maintaining the higher mechanical properties achieved by the heated cure. This was found after several

experimental parts showed a large void content with only a heated cure indicating that the part cured faster than the trapped air could escape under vacuum.

Laminate Properties

A straight forward approach to calculating a laminate's physical properties if the constituent properties and volume fractions are know is rule of mixtures. Rule of mixtures uses the fiber-volume fraction (V_f), matrix-volume fraction (V_m) and the void-volume fraction (V_v) as shown in Equation 21. The void volume represents voids due to the manufacturing process and decreases physical properties. In an ideal setting the void volume would be zero. Assuming a void free composite Equation 21 can be applied to multiple properties to calculate laminate properties based on the amount of resin and fiber used in manufacturing. The epoxy and carbon fiber reinforcement were measured by weight during the manufacturing process and the densities were used to calculate the V_f and V_m. The densities used for the prediction of mechanical properties as well controlling the ratio of reinforcement to matrix were 1.8 g/cm^3 and 1.1 g/cm^3 respectively.

Equation 21: Rule of Mixtures

$$V_f + V_m + V_v = 1$$

For this research a V_f of 50% was targeted. Due to the wet-out properties of the different carbon fibers used and the hand-layup process, this V_f was targeted as a realistic high end without having dry spots in the composite. When initially calculating the properties of the composite the void fraction was assumed to be zero although this will be shown to be an inaccurate assumption in a later section. The equations, based on rule of mixtures, used to predict laminate properties are as follows [4]:

Equation 22: Rule of mixtures: density

$$\rho_c = V_f \rho_f + V_m \rho_m$$

Equation 23: Rule of mixtures: Young's modulus

$$E_c = V_f E_f + V_m E_m$$

Equation 24: Rule of mixtures: Poisson's Ratio

$$\nu_c = V_f \nu_f + V_m \nu_m$$

Equation 25: Rule of Mixtures: shear modulus

$$G_c = \frac{1}{\left[\frac{V_f}{G_f} + \frac{V_m}{G_m}\right]}$$

Since the shear modulus of PYROFIL™ TR30S 3K is not listed by the manufacturer a similar fiber, AS4 from Hexcel, was used to estimate the shear modulus of the fiber. AS4 has similar values to the TR30S fiber but has a slightly higher tensile strength and slightly lower tensile modulus. The rule of mixtures was used to predict laminate properties. It was then compared to a composite modeling software produced by Autodesk called Helius Composite. The calculated value for $G_{t,r}$ was 2.43 GPa using Equation 25.

Helius Composite

Helius Composite can calculate laminate properties from micromechanics given the constituent material properties and fiber volume fraction. The software also has the ability to build fabrics as fabrics have different properties than unidirectional layers. This is due to the fabrics having different orientations of fibers and weave patterns that can cause crimp which reduce some of the mechanical properties of the laminate. When using Helius the void content can also be changed so that the user is able to understand how increasing the void content will affect the mechanical properties of the laminate. It has been shown that an increase in void content has the greatest effect on transverse properties with up to a 1.5% decrease in transverse modulus with every 1% increase in void content

[23]. The predicted laminate properties for the biaxial braid from Helius are given in Table 5. Note that these properties assume a 0% void content.

Table 5: Calculated properties for TR30s Biaxial Braid

TR30S Biaxial Braid (±45° plain weave)		
Property	Value	Unit
V_f	0.492	NA
Thickness	0.32	Mm
E_{11}	12.04	GPa
E_{22}	12.04	GPa
E_{33}	6.06	GPa
G_{12}	29.71	GPa
G_{13}	2871	MPa
G_{23}	2871	MPa
v_{11}	0.806	NA
v_{13}	0.077	NA
v_{23}	0.077	NA
$+S_1,S_2$	2169	MPa
$-S_1, S_2$	-1357	MPa
S_{12}	700	MPa
P	1.47	g/cm^3

NX Composite FEM Materials

Siemens NX structural finite element methods (FEM) software has a third tool that allows the user to construct laminates made from both randomly oriented fibers and different fabrics. The NX software is by far the most complex material modeling method of the three mentioned in this research and gives the user the ability to construct every element of a fully anisotropic material. This software was used in conjunction with Helius when building the FEM models used to predict failure in the composite. It was necessary to use Helius to gain a basic understanding of how the properties were generated and general ranges the properties should be in and then move to the more advanced NX system. Ultimately the properties found in Helius gave a strong starting point for the NX FEM models

and sped up the NX material modeling process. The NX FEM models will be discussed in greater detail in future sections.

Spline Shaft Revisited

With the appropriate material models the spline shaft design can be revisited and completed. Using Equation 14 with the calculated $G_{t,r}$ gives a stiffness value ($k_{t,r}$) of approximately 9200 N•m^2. When compared with a typical steel (80 GPa shear modulus) the composite teeth are approximately 33 times less stiff, but if manufactured correctly should transfer the designed loads into the tube body.

Combining Equation 15 and Equation 16 allows for the thickness of the tube to be solved for. With the thickness *t* known the number of plies can be solved for given the manufacturer's specification of a biaxial braid's thickness of 0.33 mm at 50% Vf. Since the number of plies is by whole numbers only the user must round up to the nearest whole number to ensure the design meets the equation's specifications. The wall thickness and number of plies required are 0.615 mm and 2 respectively. Since only biaxial braid was used and the material properties contained estimates, 4 layers of biaxial braid were used in the final design giving a wall thickness of approximately 1.32 mm. When designing a composite torque tube and the material for the torque tube it is beneficial to try to increase both allowable angle of twist and shear modulus as they will decrease wall thickness and therefore the torque tubes weight. Angle of twist is a less flexible variable when compared to shear modulus as it is directly related to the allowable strain in a fiber as it is being loaded. Since most carbon fibers are limited to 1-2% elongation before failure the main way angle of twist can be changed is through geometry. In this design case the geometry is fairly fixed which limits the ability to change angle of twist. Shear modulus, however, is related to both the constituent material properties as well as the fiber orientation in the ply. These tools allow the designer to utilize the anisotropic nature of the composite in

an attempt to maximize shear modulus, which is why a ±45° braid has been reiterated as a desirable material option in this design case.

FEM

As previously mentioned, Siemen's NX was used to create FEM of the composite laminate that was used to run a structural finite element analysis of the different load cases. Developing a FEM for the part was useful in comparing the results from the previous models to a simulated scenario that matched the physical inputs of the test rig and the structure of the manufactured composite. To build a laminate model in NX the first step to create useable solid body geometry that would represent the physical component.

Solid Body Modeling

To do this the solid body from Autodesk was imported and then slightly modified to separate the teeth from the torque tube as shown in Figure 15. This is a critical step that allows different properties to be assigned to the separate bodies which helps match the actual construction of the composite. With multiple solid bodies different meshes can also be applied to each one individually. This allows the user to test different the different available meshing processes for laminates in NX without using as much computing resources. When the appropriate mesh is then found it can be applied to the other solid bodies (in this case teeth) when the final simulation is to be run. The solid body modeling also modified the edge interface between the spline teeth and the torque tube. This modification simplified the geometric interface by eliminating the small fillet. The curvature of the fillet required an extremely small mesh that drastically increased the computational resources required. Since the solid bodies were already separated from each other at this point it was determined the impact of removing

the fillet would be significantly outweighed by decrease in computational time. The solid body model of the torque tube was designed to reflect the thickness of the torque tube with the theoretical thickness of the composite layers. This was a parameter that could be easily varied if the user decided to change the amount of plies in the composite.

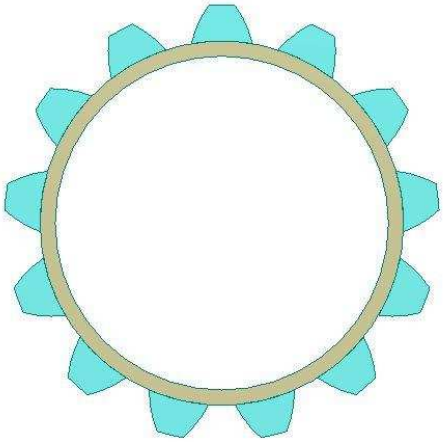

Figure 15: End view of solid body with simplified geometry for analysis

Meshing

There a couple options for meshes when using NX to model laminates with finite elements. The first option is to create a 2D mesh that maps a surface and is then either used as a 2D layer (good for analysis of plate type geometry with homogeneous properties throughout the composite where only plane stress is present) or used to generate a 3D mesh. For the spline teeth specifically a 2D quadrilateral four node mesh was applied to the tooth end face as shown in Figure 16 (a). This mesh was then used to create a 3D swept mesh through the solid along the length of the tooth (Figure 16 (b)). This approach was justified due to the nature of the composite making up the tooth and the loads exhibited there. As shown in Figure 11 there is a distributed pressure over the spline tooth. The involute geometry means that the loads act in different vectors across the involute profile. This creates out of plane forces,

which is one of the reasons for using randomly oriented fibers in the tooth. The out of plane forces are also modeled more accurately by 3D elements in Nastran, which is the solver used for laminate analysis in NX [24].

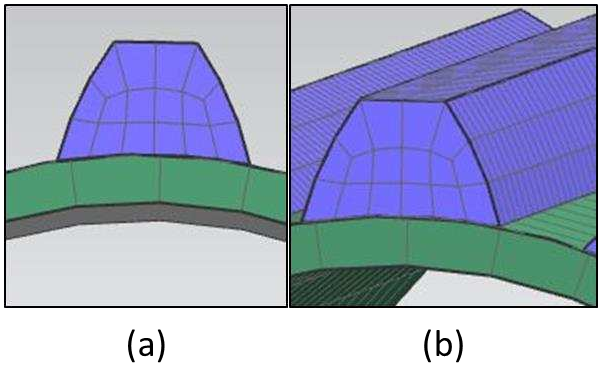

Figure 16: Tooth mesh face (a) and swept mesh (b)

To successfully model laminates in NX all of the elements must meet the NX laminate modeling requirements. Depending on the 2D structure used the elements must match the corresponding 3D structure. In the case of the tooth the mesh had to be sized and restricted to keep 2D triangular elements from forming in the otherwise quadrilateral element mesh. When extruded through the thickness of the tooth triangular elements tend to generate 5 sided penta elements which are not compatible with laminate modeling and the 8 node CHEXA elements generated by the sweep. The quadrilateral and swept elements are clearly visible in Figure 16b.

The torque tube body was modeled with the same 3D swept elements as the teeth. If only the torque tube was being analyzed it would likely be sufficient to rely on a 2D mesh and make plane stress assumptions. Since the stress is being transferred from the teeth which are modeled as a separate body and there are changes in material properties and fiber orientations at the interface 3D elements were used. These elements, as shown in Figure 16, are generated on the tube edge and swept through the body to the opposite face.

Laminate Model

With the separate bodies meshed, laminate properties can be assigned to a collection of meshes. This simplifies the phase of property assignment where there are multiple meshes with the same material properties such as the splines. The collection was assigned as a solid laminate which restricts the type of solver that can be used during calculations and allows for a solid laminate to be created. To create a solid laminate the orientation is first set for the ply sequence. For the teeth the axial direction was aligned with the X axis, or the longitudinal axis of the tube. The stack direction was aligned in the Z direction as shown in Figure 17. It is also important to note that the primary fiber direction is aligned with the x axis of the lay-up coordinate system.

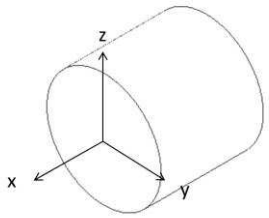

Figure 17: Lay-up coordinate system

Since the teeth are a single layer of random chopped fiber and modeled as quasi-isotropic the ply alignment has less affect since the properties are relatively the same in all directions. Next a ply was generated and assigned the random short fiber composite material properties. These properties were generated in NX's laminate ply material builder. In the builder it is possible to create a new constituent material, which was done for both the reinforcement and matrix, and then combine them in the builder. The builder has options to build unidirectional, woven, and randomly oriented fiber laminates. It also gives the ability to tailor the V_f and V_m. The rest of the properties are calculated based on the input materials.

The biaxial weave was also created in this manner. To create a weave the user must select the fiber used for both the weft and weave, which allows for different fibers to be used within the same laminate, the balance coefficient, and the fiber angle. These determine the style of weave and the orientation of the fibers with respect to each other. Since the fibers in the weave are at ±45° the fiber angle was set at 90° and the balance coefficient was set at 0.5, which means half of the fibers run at each angle. To generate the material properties for both the short fibers and the fibers used in the braid, material properties from the manufacturer were supplemented by similar materials to ensure that a complete model was used. In total the inputs to the material model were characterized by nine elastic constants for each of the constituent materials.

FEM Assembly

The full test rig design will be explained in further detail in a following section, but its main function was to apply torsion to the test sample until failure. The test rig used two splined couplings (the same used for the molds), one as the torsion applicator and one as a fixed receptor. The applicator was supported by a large bearing while the other was fixed to rigid plate. The load applicator had a hexagonal head fixed to it which allowed a large socket and torque wrench to apply the test load. To model this in NX the coupling solid geometry was imported (2 instances) and assigned 3D tetrahedral meshes and AISI 1005 Steel (approximately the actual material type) properties. The mesh and solid body can be seen in Figure 18.

Figure 18: Splined coupling with mesh

The couplings and splined shaft were then assembled in a single NX simulation using glue constraints in the areas where the shaft's teeth were engaged with the couplings. Since the shaft was manufactured in couplings the same as those used in testing the fit was quite tight suggesting that a glued constraint was actually representative of the actual assembly.

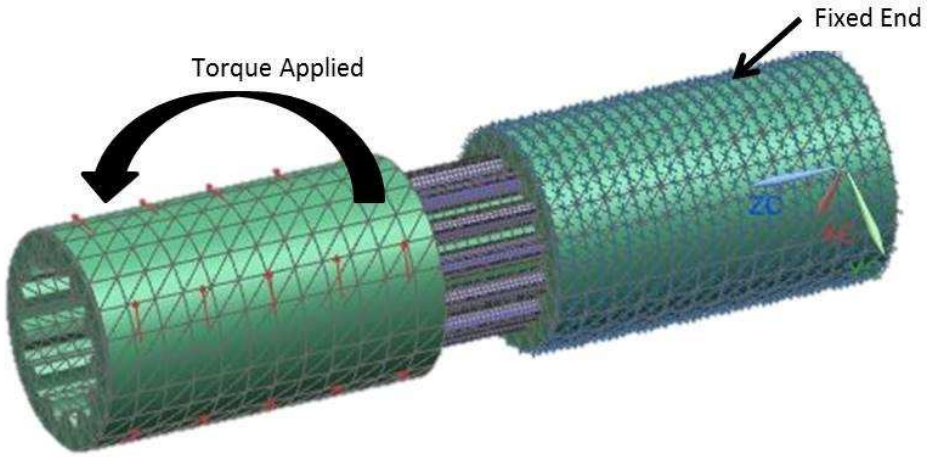

Figure 19: Full FEM assembly

A torsional load was applied to the coupling on the left of Figure 19 while a fixed constraint was applied to the right hand coupling. This again was representative of the actual loading that occurred in the test rig.

FEM Results

The simulation outputs a variety of results that help develop an understanding of how the item will fail under the test load including the visual representation of displacement (Figure 20). There are a variety of ply failure theories that can be used in the modeling software such as Tsai-Wu, maximum strain, maximum stress, and others. When comparing the failure index between different ply failure theories the spline generally fails in the same location but with varying failure indices (Figure 21). For this modeling Tsai-Wu was chosen as a failure theory since it can be used for a laminate that is generally under plane stress with unequal compressive and tensile strengths which fits the loading and design cases presented here.

The failure indices indicate that there should be failure in the tube body throughout all of the plies given 550 Nm load case. Given the material shear stress bond values for interlaminar bonding NX does not predict an interlaminar failure in the torque tube body. The software does predict failure along the root of the teeth as well as delamination of the teeth to the body depending on the interlaminar bond strength used. If the fibers in the teeth are not expected to interact with the fibers in the body then the maximum shear bonding stress should be limited to the shear stress of the matrix material. In this case the model predicts an interlaminar failure of the teeth at the root of the spline (Figure 22). If different shear bond strength is used in an effort to model the co-molding interaction then the failure indices for this are reduced to show little chance of failure.

Figure 20: Visual scaled displacement of the splined shaft

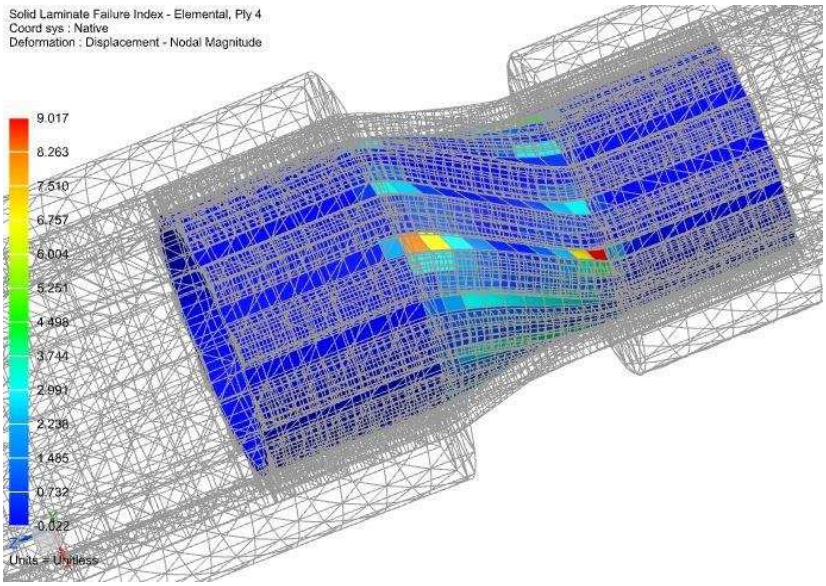

Figure 21: Solid laminate failure index for ply 4 of the torque tube body

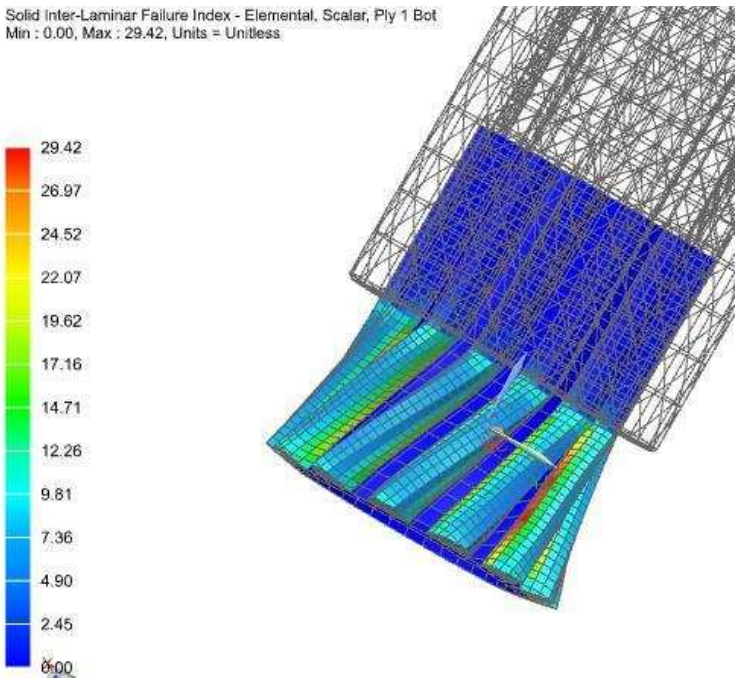

Figure 22: Interlaminar failure index of the spline teeth to the body using the bond strength of the epoxy

SPLINE SHAFT MANUFACTURING

The spline shafts were manufactured in a multi-step singe cure hand lay-up process. There were three phases of the manufacturing process, each representing a major refinement or change in process to improve the final part quality and reduce manufacturing time. The phases are represented by sample number with the first phase starting at sample A1, the second at A7, and the third and final phase at A11.

Phase One

Material Preparation

The first phase of manufacturing was intended to provide a proof of concept that the manufacturing plan was valid. The manufacturing plan was to use the spline coupling as a mold, create a bulk molding compound from the random short fibers and epoxy, fill the teeth with the compound and then finish by laying-up the biaxial braid. The curing process was to be a full room temp cure under vacuum for a minimum of six hours. Empirically after six hours very little gases can be extracted by the vacuum due to the change in viscosity of the epoxy matrix. The volume of the bulk molding compound was estimated by calculating the volume of the spline cavities using a trapezoidal approximation shown in Figure 23.

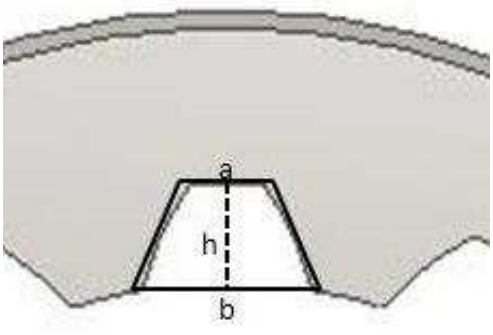

Figure 23: Trapezoidal approximation

Calculating the area of the trapezoid shown in Figure 23 using length approximations measured from the actual coupling and multiplying it by the length of the spline gave a reasonably accurate spline tooth volume. Multiplying this value by the number of splines gave the total volume of bulk molding compound required to manufacture all 13 splines. Using a V_f of 50%, the rule of mixtures equations previously listed, and the densities of the matrix and reinforcements allowed for a back calculation of much reinforcement and matrix were needed, by mass. Roughly 23g of ¼'' chopped carbon fiber and about 12g of mixed epoxy filled the required volume. Since the stoichiometric ratio for mixing the epoxy is 33phr by mass, the total amount of hardener and resin can be found if the final mass is known.

The braid takes less calculation as it can be measured and cut in its dry form and compared to the mold to ensure a proper fit. Since each layer is slightly shorter than the previous to account for the change in diameter throughout the layers each on is laid out in order before manufacturing so that they are laid up in the correct order. After each layer is cut they are weighed so that the correct amount of matrix, by mass, can be mixed to create a 50% V_f. The epoxy used is the same for both the biaxial braid and the random short fibers as is the resin to hardener ratio.

To cure the wet lay-up under vacuum, a vacuum bagging system must be set up. For these samples a super elastic vacuum bagging material was purchased. This vacuum bagging material is more

suited for this application since it must be pliable enough to conform around the mold without having vacuum leaks. The bagging material was cut into strips that were approximately 25 cm long and 14 cm wide. Double sided vacuum bagging tape was then placed along the long edge of the bagging material with approximately half of the width of the tape hanging over the edge. The bagging material was then folded over to create an open ended tube sealed internally by bagging tape as shown in Figure 24.

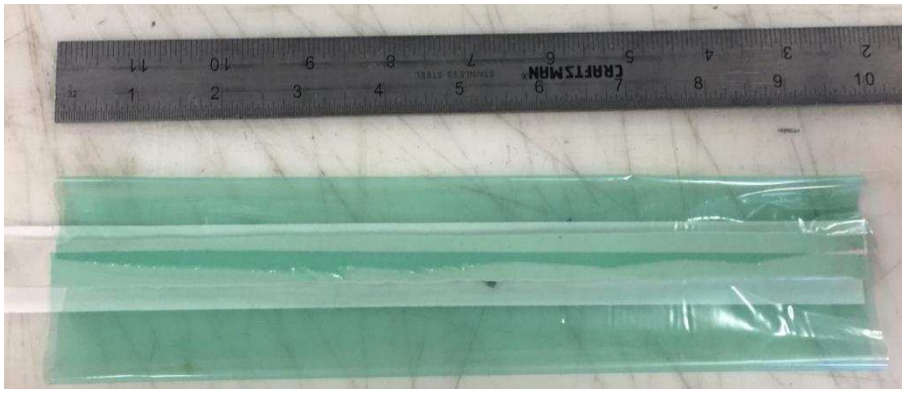

Figure 24: Internal bagging tape

The diameter of the tube shown in Figure 24 is approximately the same as the internal diameter of the part with four layers of biaxial braid. The diameters were closely matched to try and avoid wrinkles and gaps between the bagging and the part that could potentially draw resin into them. This section of the bagging material is used to provide pressure against the internal walls of the mold consolidating the different layers of composites while the vacuum removes trapped voids.

To complete the seal a larger rectangle was cut out of the bagging material and lined on three sides with the bagging tape. This created a pouch that could fold over the ends of the tube shown in Figure 24 to complete the seal all the way around. A Toray quick release vacuum port was used to provide vacuum once the lay-up was complete. All of the materials used in the lay-up process, except for

the epoxy, were compiled into ready to use kits (Figure 25). These kits included a waxed mold, pre-weighed chopped and biaxial fiber enclosed in sealed bags to keep out debris, cut breather, release layer, and bagging material. Starting in phase two the kits were made in bulk to decrease work time during the lay-up process.

Figure 25: Lay-up kit

Lay-up Process

The lay-up process started with the cleaning of the couplings. From the manufacturer the couplings came with a light oil fil on them which could negatively affect the composite. They were cleaned with a solvent and allowed to dry. A mold-release wax was then applied to the outer and inner surfaces of the tooling. The release layer helps prevent the composite from adhering to the mold during cure as well as protects it from the elements. Initially four release coats were applied where each coat was allowed to dry and was then buffed off as per manufacturer directions. After the first application only one to two release coats were applied to the internal splines between lay-ups. With the molds

prepped before lay-up and all of the fibers pre-measured (both braid and chopped fiber) the chopped fiber could be mixed with the epoxy to create a bulk molding compound.

The epoxy hardener and resin to be used with the chopped fiber were measured into a disposable cup and thoroughly mixed. They were allowed to sit for a few minutes and then re-mixed again to help ensure full mixing and to let some of the air escape. Chopped fibers were then slowly mixed in to ensure full fiber wet-out. This was quite difficult due to the large amount of loose fibers and fiber area compared to epoxy. Most bulk molding compounds have a much lower fiber volume fraction than the one used for this project [4]. With the fibers fully mixed in the phase one manufacturing process called for packing the spline teeth with the compound. For this phase, all of the compound was used at once and packed into the teeth as much as possible. The next step was mixing the final batch of epoxy to be used with the biaxial braid. A small diameter plastic sleeve had epoxy placed on it and then the biaxial braid was slipped over the sleeve. Squeegees were used to draw the epoxy up through the braid to ensure full wet-out. The four layers of biaxial braid were laid up over each other and elongated to reduce their diameter as much as possible. With a smaller diameter they could be inserted inside the mold with more ease. The plastic sleeve was removed and the braid was expanded in the mold. The bagging material was placed around the lay-up and fully sealed and vacuum was applied for the duration.

Problems identified with phase one were related to the amount of time and difficulty in placing the bulk molding compound in the molds. Applying the bulk molding compound to the mold all at once caused a large amount of displaced fibers which tended to catch on the biaxial braid and shift the fibers out of the teeth. It was observed that shifting the fibers after placement tended to cause large voids and inconsistent cross sections since there would be more material in one spot after it shifted. After a few

attempts at processing in this manner phase two was developed to help reduce stray fibers and increase the part quality.

Phase Two

The second phase of manufacturing was characterized by a change in the lay-up process to increase part quality and ease of manufacturing. Examining the cured parts showed a need for consistency in the amount of chopped fiber used in each spline. By packing it in all at once there was not an even distribution of bulk molding compound in each of the teeth cavities. This showed up in the finished part as lumps and voids. It was also noted that the time it took to mix in all of the fibers and lay them up was quite long and the epoxy resin was starting to reach the end of its workable pot life by the time the biaxial braid was laid up. This was also having an impact on part quality since the compound was less moldable by the time the braid was inserted in the mold and shifting the molding compound would decrease part quality.

To remedy these issues bulk molding compound charges were used. Essentially all the molding compound was put on a clean sheet and then divided evenly into 13 pieces. Dividing up the molding compound was done by hand at this point and the charge weights were not measured, just estimated by visual size and feel. These charges were then roughly shaped to fit the teeth cavity of the mold. The mold was then coated with a thin layer of epoxy to help increase surface finish and keep the fibers from drying out under vacuum. Once the mold was coated the charges were packed into the teeth cavities and pressed down with a clean rod or mixing stick. The braid process remained unchanged but went much faster and smoother since the molding compound charges had significantly less loose fibers protruding randomly (Figure 26).

Figure 26: Molding compound charges

Instead of doing a full room temperature cure at this point the cure cycle was changed to help increase some of the properties of the matrix. This particular resin and hardener system crosslinks more when it is cured with heat (100° C for one hour) increasing most of its physical properties. Several of the phase two parts were cured completely under vacuum in the oven using a 2° C ramp per minute with a one hour hold at 100°C. The parts were then allowed to air cool before removing them from the molds.

The changes in manufacturing made the lay-up process more straight forward and with less complications. The charges were successful in reducing stray fibers and fiber shift in the bulk molding compound by interacting less with the biaxial braid during lay-up. This helped reduce the amount of displaced fiber and increased the consistency of compound quantity across the spline teeth. The change in cure cycle had detrimental effects to the part quality. Since the cure cycle was so quick there were noticeable voids in the part where the trapped air did not have time to travel through the part under vacuum. The issues described in phase two manufacturing are visible in Figure 27.

Figure 27: Phase two sample with poor surface finish and voids (red circle)

Phase Three

The final phase of manufacturing improved several aspects of the process and increased part quality to an acceptable level and was a highly repeatable process. Since the cure cycle in phase two was causing issues it was changed to a room temperature cure followed by a post cure. The room temperature cure was performed under vacuum for 4-6 hours after which vacuum was removed and the phase two heated cure was used. The other main change was splitting the bulk molding compound process into two parts and refining the process by weighing each charge individually. Splitting the charge process into two steps meant separating the dry chopped fiber and epoxy into two equal portions before mixing. This allowed for an easier mixing process since less dry fiber was used even though the ratio was the same. The larger amount of fibers was more difficult since they tended to stick together in one large ball during mixing. This actually decreased processing time as well since the mixing process went significantly faster as a split process. Weighing all of the charges ensured that the charge size was in an appropriate range for each spline tooth which helped create a more uniform part. Processing was further improved by adding slightly more breather and release layer between the bagging material and the part. The changes in phase three produced a more repeatable and higher quality part as shown in

Figure 28. This part has a relatively consistent cross section, few surface voids, few exposed voids on the splined ends, and a smooth surface finish. The sample in Figure 28 is the first part from the phase three manufacturing.

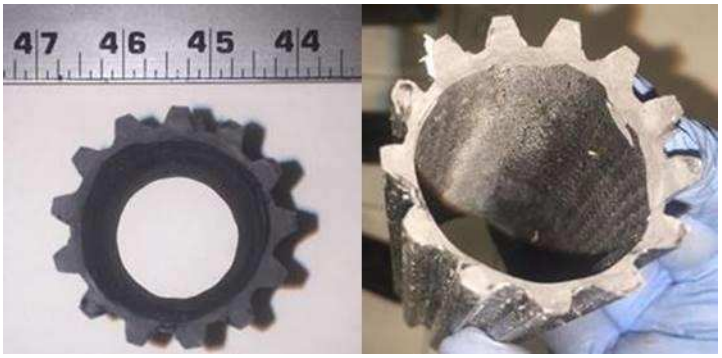

Figure 28: Sample from phase three manufacturing

To increase fidelity in data collection another step that was added was the weighing of the mixing cups used for resin mixing before and after lay-up. Knowing the mass of the disposable mixing cup before mixing resin allows for the user to understand how much resin is lost between mixing and lay-up. Since the ratios were calculated to be exactly a 50% V_f initially, any resin not used in the process changes the final V_f. Although losing resin should increase the V_f, which can increase the physical properties, it can also lead to dry areas in the composite. In the wet lay-up process it can be difficult to adequately wet-out all of the fibers depending on the amount of resin used. Aiming for a higher V_f in the composite can ultimately leaded to dry areas which can't effectively transfer load between the fibers. This acts as a load concentrator and can lead to pre-mature failures. Weighing the cups allowed for the lost resin to be accounted for in the data analysis section and influenced the measuring of the epoxy to generally err on the side of slightly too much epoxy than not enough.

Post Processing

Post processing was required to remove the spline shaft from the mold as well as use it in the testing apparatus. Due to the vacuum bagging method some loose fibers tended to extrude past the end of the mold and cure around the edges of the tooling. This created a physical trap where the rest of the shaft could not be removed since it was caught on both edges of the tooling (Figure 29).

Figure 29: Composite in tooling

To help remove the shaft from the mold a Dremel tool was used to cut and sand the edges of the spline shaft down to the interior surface of the mold. This resulted in the interiorly angled spline teeth shown in Figure 30.

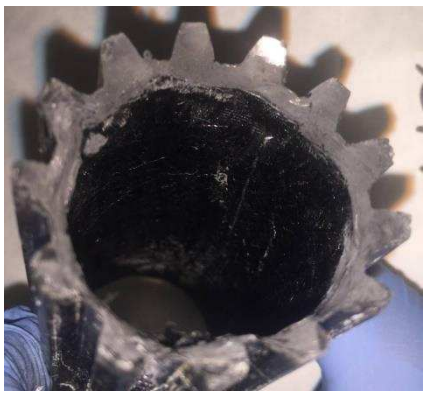

Figure 30: Post processed splined shaft with interiorly angled teeth

Since the teeth on the tooling were steel they could be used as a processing jig so that every spline was trimmed to the same final shape and length. The coupling and shaft were also placed in the freezer for several hours to help separate the two pieces from each other. The cooling of the steel increased the inner diameter while the carbon piece stayed relatively the same size. These slight differences in size helped remove the part while minimizing damage to both the tooling and the finished composite. To remove the composite part from the mold the male steel spline shaft was used as a punch and tapped through the coupling forcing the part out the other end. Since the steel shaft was mated to the coupling the splines acted as guides. The end of the shaft was also chamfered at the same angle as the interiorly angled teeth so that it rested snugly against the composite.

TESTING

This section will focus on the test fixture design and manufacturing and then discuss how the testing was conducted. The test fixture includes the physical test apparatus as well as the instrumentation utilized to collect data and how it was calibrated.

Fixture Design Criteria

The test fixture needed to satisfy the design objectives listed below:

1. Apply pure torsion to the spline tubes
2. Hold the samples in the same position through the series of testing
3. Be rigid and strong enough to accept loads up to 1000 Nm
4. Record or output results

Although the design was broken down into four objectives most of them require multiple inputs to be achieved. To apply pure torsion to the spline tubes one end must be fixed and the other end supported by some sort of bearing so that the sample doesn't experience bending or other non-torsional forces. For one end to be fixed the fixture is required to have a fixed female spline that matches the shaft. The same is true to apply load, except the female spline must be free to move when torsion is applied. This means that the female spline used to apply the load, in this case called the applicator coupling, also needed to be supported by a bearing. Since the female couplings were already defined during tooling and used to create the parts the same parts could be used in testing. The couplings, however, are completely smooth on the outer surface which creates the issue of actually transferring torque into the applicator coupling. Another issue with transferring torque is the high

torque needed to be transferred (up to 1000 Nm to ensure part failure). Since there was no obvious mechanism for torque transfer one needed to be developed.

To hold all of the samples in the same position a method for applicator and receptor coupling alignment was needed. A method for sample removal and placement was also required which indicated that either the applicator or the receptor coupling and related fixtures would be required to move. This was assumed since the spline shaft and couplings had a tighter fit than a usual shaft and coupling pair would because the part was made to the dimensions of the coupling mold.

Fixture Design

With much of the criteria known the initial design was sketched up by hand. This design included a fixed coupling acceptor, a coupling acceptor in a bearing and a clamp system with machined flats so that a wrench (lever arm) could apply torque to the system. The acceptor coupling and bearing system was drawn on a sliding system so that the distance could be adjusted and the spline shaft removed. When exploring standardized components to meet these needs the bearings were the most restrictive. With an outside diameter of roughly 63.5 mm the couplings limited the bearing choices significantly. There were some options for roller bearings this size, but then a bearing housing would need to be machined which would require a significant amount of time and resources. To save on time and materials a pillow block roller bearing was sourced that fit the coupling. Ideally two roller bearings would be used to fully support the applicator coupling but since the bearing race so large only one bearing could be used. The pillow block had pre-drilled holes in its supports which dictated width of the sliding system to be used.

While searching for standardized equipment a torque wrench multiplier with a 4:1 multiplication ratio was sourced. This when paired with a 250 Nm capable torque wrench would achieve

the desired 1000 Nm of torque. To use this, a socket (instead of a wrench) would need to be used to transfer the load to the applicator coupling. The smallest six-point socket available that would fit with the other components was a 2.5'' impact socket. To be able to use this, the design was changed to include a hex stock adapter. The adapter was a 2.5'' section of hex stock blind bored to the outer diameter of the applicator coupling. To easily attach the hex stock to the applicator coupling, holes were drilled on each of the six faces of the hex stock. The applicator coupling was inserted into the bored section of hex stock and through holes were drilled through each hole. These six holes were then through-tapped so that bolts could be used to fix the hex stock to the coupling. These modifications finished the torque application section of the test fixture.

The torque receptor section of the design did not require movement but needed to be strong and stiff enough to avoid deflecting or breaking under load so as to not affect the results of the torsion tests. To mount the steel receptor coupling two part clamps attached by bolts were used. The clamps were purchased with machined flats in them which allowed them to stand flat against a steel plate. To locate them on the steel plate holes were drilled and tapped into the plate in the desired pattern and to match the bolts from the clamps. The clamps were then bolted to the plate and tack welded in place. Once the tack welding was completed the bolts were removed and the clamp bases were fully welded. The coupling was then welded to the clamps. The steel base plate was drilled with mounting holes as well.

To complete the structure a large steel base plate was water jetted with slots and mounting points so that the two systems could be mounted and aligned with each other. To align the heights shims were machined to lift the receptor coupling so that the center heights aligned. To test alignment the original steel splined shaft was used as well as visually aligning. During testing, to align the system the bearing was loosened from the slots so it could freely move. The test sample was placed in the

applicator coupling and then aligned with the receptor coupling. As the test sample was inserted into the receptor coupling the bearing would shift and self-align. The full CAD of the test set-up can be found in Figure 35 of Appendix D.

Measurement

The primary interest in this research was examining the torsional load capacity of a composite splined coupling. The data collected for this research was ultimate torsional load and a visual inspection of the part failures. Torsional load was collected in two methods: from the digital torque wrench and from an S-type load cell. The digital torque wrench output a maximum torque value applied once the load had been released. This value was recorded for each sample along with notes about the test and the failure. The load cell was wired to an amplifier and the system was calibrated using pre-measured weights. The calibration provided the information to generate a function to calculate load based on voltage output. The output signal was wired to an Arduino analog input which output the voltage to a data file. The sample rate for this was approximately every 0.25 seconds to help ensure the maximum load would be recorded. The voltage reading was then used to calculate the vertical load on the load cell which in turn was used to calculate torsional load based on the moment arm length. Both of these measurement systems gave torsional values that were pre-multiplier head. Ideally the moment arm on the multiplier head would have output values of the multiplied torque to understand the losses in the multiplier but this was not the case.

Testing

The testing was done in a repeatable process that could be verified by simple measurement tools. Each part was marked with insert lines for both the receptor coupling and applicator coupling. This allowed for the same amount of spline engagement in both couplings across all of the parts. To ensure that the loads were applied the same the hex adaptor was marked in relation to the applicator coupling so it could be attached the same each time. The torque multiplier handle was marked and located on the load cell in the same position for each test and the torque wrench was positioned in the same initial position for each test as well. Each test was documented with notes and pre and posttest photos to help ensure consistency across testing. It should be noted that there was some slight variation in the location of the multiplier handle as it had some play in the connection to the head.

RESULTS

Data Set

The collected data varied between the torque wrench digital output and the calculated torque from the load cell by a significant amount (always higher). This could be due to calibration error or the interaction between the lever arm and the load cell. Since the recorded values were always higher the lower range (which were from a high grade factory calibrated torque wrench) they were not treated as valid results. T samples failed quality checks from manufacturing but were tested anyways (sample A5, A6) so the data from these samples was truncated from the sample set. Sample A8's was not tested since it required additional post processing to fit the test rig (sanding of spline surfaces). Samples A1 and A2 were not tested since they were cut to examine the cross section to inform further manufacturing decisions. This left a sample set labeled from A3 to A20, excluding the truncated items, where phase three manufacturing started with sample A11. The recorded failure torque values, pre and post (calculated) multiplier head are found in Table 6. The average failure torque (no de-rating) is approximately 574 N-m across the phase three samples which agrees with the FEM model, but not with the torque tube analysis which should fail around 1000 Nm with four layers. This is likely due to the assumption the torque tube model analysis makes of treating it as a solid body instead of four individual layers when in fact the interlaminar properties have a large effect on the properties of the overall laminate.

Table 6: Torsion test results in Nm; 4x multiplier with no derating

Torsion Test Results (Nm)															
Sample	A3	A4	A7	A9	A10	A11	A12	A13	A14	A15	A16	A17	A18	A19	A20
Raw Torque	91.2	77.5	156	107.6	98.3	251.3	160.2	184.6	99.3	142.8	131.8	131.1	85.4	141.9	107.4
Multiplied Torque	364.8	310	624	430.4	393.2	1005.2	640.8	738.4	397.2	571.2	527.2	524.4	341.6	567.6	429.6

Failure Modes

A majority of the samples had the same primary failure mode which was a failure at 45° to the tube axis in the tube body. The failures ran parallel to half the fibers and perpendicular to the others as shown in Figure 31.

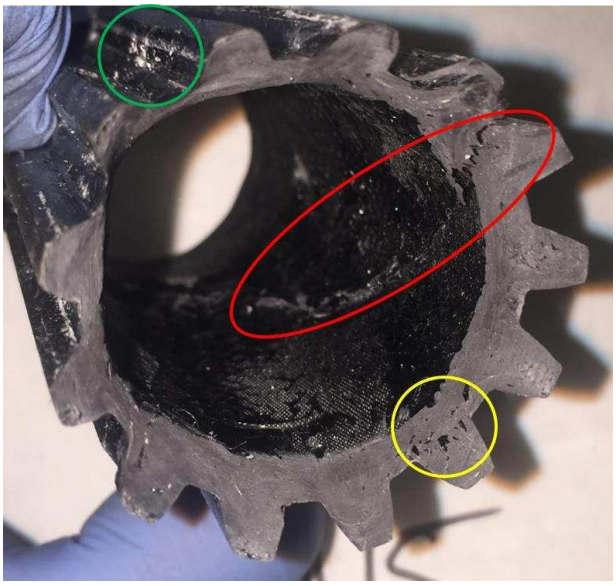

Figure 31: Sample A15 after testing showing spline damage (green), main tube failure (red), and porosity (yellow)

Another common failure which was not identified as the primary form of failure was segments of delamination of the teeth from the main body. This is shown in the green circle in Figure 31 and in more detail in Figure 32. This failure was not identified as the primary failure in any of the samples since there were samples with minor to no visible delamination at failure and in the samples with tooth separation there was always the presence of the fracture in the main body. Since stress in the composite is transferred by shear mechanisms it seems likely that the teeth started to shear from the tube body under load. Sample A11 had the highest failure load and also exhibited some of the largest delamination suggesting that there is a practical upper limit at which the teeth are capable of transferring the load into the main body.

Figure 32: Sample A11 after testing showing separation of teeth from body (green)

Some samples showed fractures through the teeth which was characterized as different from delamination. These failures did not occur in every sample but often stemmed from the boundary between the edge of the steel couplings and the sample. Figure 33 clearly shows the different types of tooth fracture (often multiple fracture lines) stemming from the coupling mounting locations. The stress concentrations from the end of the couplings likely caused the various fractures here and will probably continue to be an issue in design if composite spline shafts are used with metal couplings. Also visible on almost all of the samples are bite marks from the couplings which support the idea of stress concentrators.

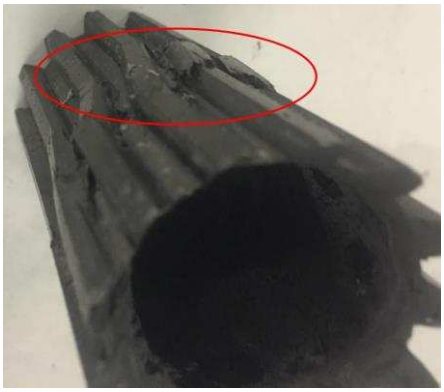

Figure 33: Sample A20 after testing showing fractures in teeth (red)

CONCLUSIONS

The research conducted to understand the feasibility of using splined shaft geometry in composites advanced the understanding of the possibilities and limitations of composites in this novel application. On average the samples from phase three manufacturing failed at approximately 96% of the designed load. All of the samples exhibited a failure in the torque tube body at 45° to the tube axis indicating that load was transferred from the splines into the tube body.

Since every sample that delaminated also had failures in the tube body it can be concluded that the teeth failed after the body. Since all of the stresses are modeled as being transferred by the matrix material into the fibers if the teeth delaminated first there would be no failure in the body since the loads would no longer be transferred into that portion of the composite. This suggests that using an involute spline geometry manufactured from composites as a method for torque transfer into a composite torque tube is viable. This conclusion should hold true as long as there is enough contact area at the base of each spline to fully transfer the load into the torque tube once it is distributed by each spline. Additional research is recommended to discover what the upper limit of the torque load transfer of the teeth to the tube is given the same loading scenario. This is directly affected by the interlaminar bond strength between the teeth and the fiber which is shown to be higher than just the bond strength of the epoxy. This indicates that there is some fiber interaction that is increasing this interlaminar strength between the teeth and body that was not captured in the models presented in this paper but is predicted to behave as shown in Figure 34 where the biaxial braid is actually interfacing with part of the tooth.

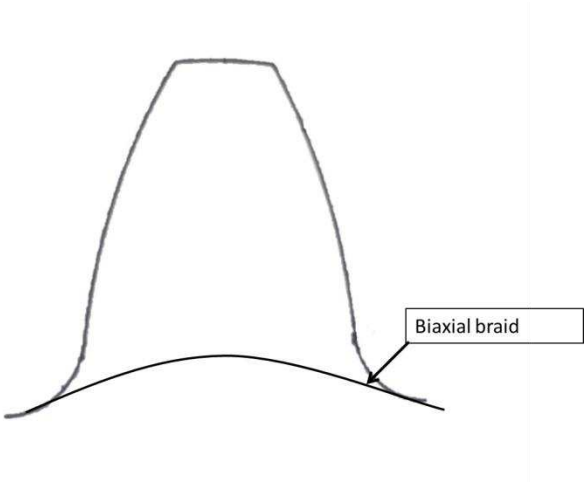

Figure 34: Predicted biaxial braid behavior when co-molded with tooth

The design case presented in this research showed that there are uses for high grade bulk molding compounds in torque transfer applications in this specific scenario. The process of co-molding the bulk compound with the biaxial braid to form a single composite has the potential to have widespread applications especially if the interface between the two sections of the spline shaft is modeled more in depth. With an increase in interface modeling for this application composite splines could have widespread applications in design, especially if the design is proved to be scalable in manufacturing and size.

Since the design holds promise as a lightweight method for torque transfer it is also suggested that additional research should be conducted to understand the design envelope restrictions. Initial design and manufacturing showed that to generate a constant velocity style shaft (a shaft with two splined ends) a multi-part mold was required and the lay-up process was much harder to maintain. In the case of expanding the design to a full double ended shaft, different methods of manufacturing such as resin transfer molding could be explored. This would increase the repeatability of the samples and the part quality. Another aspect that would be beneficial to inspect would be the development of a splined shaft that was dimensionally the same as the steel splined shaft that fit the couplings. In current

manufacturing the male and female splines do not mate as tight as the composite shaft and steel coupling. The backlash between the two components could significantly change the torsional capacity of the composite teeth as it has been shown that the teeth are loaded differently in the presence of backlash [19].

REFERENCES

[1] D. L. Greene, "Reducing Greenhouse Gas Emissions From Transportation," Oak Ridge National Laboratory, North Carolina, 2006.

[2] U. Government, "the White House," U.S. Government, 28 August 2012. [Online]. Available: https://www.whitehouse.gov/the-press-office/2012/08/28/obama-administration-finalizes-historic-545-mpg-fuel-efficiency-standard. [Accessed 29 July 2016].

[3] J. E. Duffy, Modern Automotive Technology, Tinely Park: The Goodheart-Willcox Company Inc., 2009.

[4] A. B. Strong, Fundamentals of Composites Manufacturing Materials, Methods and Applications, Dearborn: Society of Manufacturing Engineers, 2008.

[5] Composites World, "Composites World: BMW rolls out prototypes of composites-intensive i3, i8," BMW, 8th August 2011. [Online]. Available: http://www.compositesworld.com/news/bmw-rolls-out-prototypes-of-composites-intensive-i3-i8. [Accessed August 2015].

[6] B. K. Suryawanshi and P. G. Damle, "Review of Design of Hybrid Aluminum/Composite Drive Shaft for Automobile," *International Journal of Innovative Technology and Exploring Engineering,* vol. 2, no. 4, 2013.

[7] D. G. Lee, H. S. Kim, J. W. Kim and J. K. Kim, "Design and Manufacture of an automotive hybrid aluminum/composite drive shaft," *Composite Structures,* vol. 63, pp. 87-99, 2004.

[8] J. Shigley, C. Mischke and R. Budynas, Mechanical Engineering Design, 7th ed., New York: McGraw-Hill, 2004.

[9] J. E. Shigley, C. R. Mischke and T. H. Brown, Standard Handbook of Machine Design, New York: McGraw-Hill, 2004.

[10] R. R. Robins, "Tooth Engagement Evaluation of Involute Spline Copulings," Brigham Young University, Salt Lake City, 2008.

[11] D. Dudley, Handbook of Practical Gear Design, Lancaster: Technomic Publishing Inc., 1994.

[12] I. Hayashi and T. Hayashi, "Miniaturization of Involute Spline Copulings- Discussion from Torsional Stiffness and Yield Torque," *Bulletin of JSME,* vol. 28, no. 236, pp. 259-266, 1985.

[13] Fellows Corporation, "Back to Basics," *Gear Technology,* pp. 37-48, October 1984.

[14] R. Heald and C. J. McCAuley, Machinery's Handbook, New York: Industrial Press, 2004.

[15] R. S. Gross and J. G. Goree, "An Experimental and Analytical Investigation of Composite Drive Shafts with Non-Circular End Cross-Sections," *Journal of Composite Materials,* vol. 27, no. 7, pp. 702-720, 1993.

[16] A. Barrot, M. Paredes and M. Sartor, "Determining both radial pressure distribution and torsional stiffness of involute spline coupling," *Journal of Mechanical Engineering Science,* vol. 220, no. 12, pp. 1727-1738, 2006.

[17] W. Milliken and D. Milliken, Race Car Vehicle Dynamics, Warrendale: SAE International, 1995.

[18] V. Bhajantri, S. Bajantri, A. Shindolkar and S. Amarapure, "Design adn Analysis of Composite Drive Shaft," *International Journal of Research in Engineering Technology,* vol. 3, no. 3, pp. 738-745, 2014.

[19] F. Cura and A. Mura, "Analysis of a load application point in spline coupling teeth," *Journal of Zhejiang University-Science A,* vol. 15, no. 4, pp. 302-308, 2014.

[20] P. S. Steif, Mechanics of Materials, Upper Saddle River: Pearson Higher Education Inc., 2012.

[21] S. M. Andersen, "Design/Engineering with Composites," University of Delaware Center for Composite Materials, Delaware.

[22] Resolution Performance Producs, "EPON Resin Structural Reference Manual," Resolution Performance Products, 2001.

[23] C. Dong, "Effects of Process-Induced Voids on teh Properties of Fibre Reinforced Composites," *Journal of Materials Science & Technology,* vol. 32, pp. 597-604, 2015.

[24] P. Goncharov, I. Artamonov, T. Khalitov, S. Denisikhin and D. Sotnik, Engineering Analysis with NX Advanced Simulation, Lulu Publishing Services, 2014.

[25] Mitsubishi Rayon, "Pyrofil TR30S Data Sheet," Mitsubishi Rayon.

[26] Hexcel Corporation, "HewTow AS4 Carbon Fiber Product Data Sheet," Hexcel, 2016.

APPENDIX

A: Spline Data

Table 7: Spline Data

Internal Involute Spline Data		
Number of Teeth	N	13
Pressure Angle	PA	30.0 deg
Diametral Pitch	DP	8/16
Base Diameter	d_b	35.74 mm
Pitch Diameter	D_p	41.275 mm
Major Diameter (internal dedendum)	D_{ri}	44.45 mm
Minor Diameter (internal addendum)	D_i	38.10 mm
Edge Radius	r_e	0.203 mm
Flank Length	l_f	4.93 mm
Tooth thickness	t	4.90 mm
External Involute Spline Data		
Number of Teeth	N	13
Pressure Angle	PA	30.0 deg
Diametral Pitch	DP	8/16
Base Diameter	D_b	35.74 mm
Pitch Diameter	D_p	41.275 mm
Major Diameter (external addendum)	D_o	44.45 mm
Minor Diameter (external dedendum)	D_{re}	38.10 mm
Edge Radius	r_e	0.203 mm
Flank Length	l_f	4.93 mm
Tooth thickness	T	4.90 mm

B: Reinforcement Data

Table 8: Various reinforcement properties used

Braided Carbon Biaxial Sleeve		
Property	Value	Units
Nominal Diameter	38.1	Mm
Nominal Angle	±45	deg
Yield	29.7	m/kg
Fabric Weight	0.28	Kg/m^2
Thickness at 50% V_f	0.33	Mm
Tensile Strength	4.2-4.8	GPa
Tensile Modulus	214-241	GPa
Elongation	1.75-2.1	%
Pyrofil™ TR30S 3K [25]		
Tow Tensile Strength	4410	MPa
Tow Tensile Modulus	235	GPa
Density	1.79	g/cm^3
Typical Yield (3K)	200	mg/m
HexTow® AS4 Carbon Fiber 3K [26]		
Tensile Strength	4619	MPa
Tensile Modulus	231	GPa
Elongation at Failure	1.8	%
Density	1.79	g/cm^3
Yield	4.75	m/g
HexPly 8552 Composite Properties at 60% V_f [26]		
0° Tensile Strength	2205	MPa
0° Tensile Modulus	141	GPa
0° Tensile Strain	1.55	%
0° Flexural Strength	1889	MPa
0° Flexural Modulus	127	GPa
0° Short Beam Shear Strength	128	MPa
90° Tensile Strength	81	MPa

C: Matrix Data

Table 9: Epon 828/3140 unfilled casting data

Properties of 828 cured with 3140 @ 33phr		
Property	Value	Unit
Viscosity @25°C	14	Pa*s
Viscosity @40°C	0.4	Pa*s
Density	1.10	g/cm^3
Useable Pot Life	75	min
Linear Shrinkage	0.0197	mm/mm
Compressive Yield Strength	84	MPa
Tensile Yield Strength	49	MPa
Tensile Shear Strength	17	MPa
Tensile Modulus (@82phr, 23°C cure)	2100	MPa

D: Fixture Design

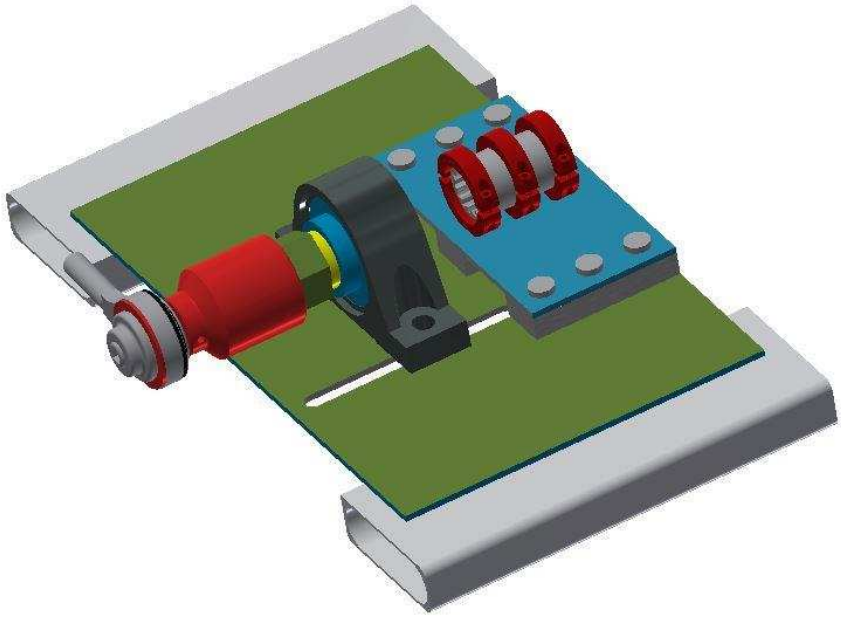

Figure 35: Full test fixture assembly CAD (not pictured are bolts mating hex stock to applicator coupling)